

Loss of CD73-mediated actin polymerization promotes endometrial tumor progression

Jessica L. Bowser,¹ Michael R. Blackburn,² Gregory L. Shipley,³ Jose G. Molina,² Kenneth Dunner Jr.,⁴ and Russell R. Broaddus⁵

¹Department of Translational Molecular Pathology, The University of Texas MD Anderson Cancer Center, Houston, Texas, USA. ²Department of Biochemistry and Molecular Biology and ³Department of Integrative Biology and Pharmacology, The University of Texas Medical School at Houston, Houston, Texas, USA. ⁴Department of Cancer Biology and ⁵Department of Pathology, The University of Texas MD Anderson Cancer Center, Houston, Texas, USA.

Ecto-5'-nucleotidase (CD73) is central to the generation of extracellular adenosine. Previous studies have highlighted a detrimental role for extracellular adenosine in cancer, as it dampens T cell-mediated immune responses. Here, we determined that, in contrast to other cancers, CD73 is markedly downregulated in poorly differentiated and advanced-stage endometrial carcinoma compared with levels in normal endometrium and low-grade tumors. In murine models, CD73 deficiency led to a loss of endometrial epithelial barrier function, and pharmacological CD73 inhibition increased in vitro migration and invasion of endometrial carcinoma cells. Given that CD73-generated adenosine is central to regulating tissue protection and physiology in normal tissues, we hypothesized that CD73-generated adenosine in endometrial carcinoma induces an innate reflex to protect epithelial integrity. CD73 associated with cell-cell contacts, filopodia, and membrane zippers, indicative of involvement in cell-cell adhesion and actin polymerization-dependent processes. We determined that CD73-generated adenosine induces cortical actin polymerization via adenosine A₁R induction of a Rho GTPase CDC42-dependent conformational change of the actin-related proteins 2 and 3 (ARP2/3) actin polymerization complex member N-WASP. Cortical F-actin elevation increased membrane E-cadherin, β -catenin, and Na⁺K⁺ ATPase. Together, these findings reveal that CD73-generated adenosine promotes epithelial integrity and suggest why loss of CD73 in endometrial cancer allows for tumor progression. Moreover, our data indicate that the role of CD73 in cancer is more complex than previously described.

Introduction

Ecto-5'-nucleotidase (NT5E, referred to herein as CD73) is a cell surface glycosylphosphatidylinositol-anchored (GPI-anchored) glycoprotein that catalyzes 5'-adenosine monophosphate (5'-AMP) to adenosine (1). CD73 is overexpressed in a number of human tumors (2), promotes tumor growth and metastasis (3–12), and is associated with drug resistance (13–15). Previous studies highlight a detrimental role for extracellular adenosine generation and signaling in cancer, specifically that of dampening T cell-mediated immune responses (3–8, 16). Unexpectedly, we found that CD73 was downregulated in poorly differentiated and advanced-stage endometrial carcinoma and ovarian high-grade serous carcinoma (HGSC), both clinically aggressive neoplasms of the female reproductive tract. Up to now, there has been little evidence to suggest that CD73-generated adenosine may act to oppose disease progression in human tumors.

In normal tissues, CD73-generated adenosine is essential for protection, as it prevents the destruction of tissue homeostasis and integrity caused by inflammation, ischemia, or hypoxia (17). In these settings, adenosine accumulates at the cell surface and induces immunosuppression (18), angiogenesis (19), mucosal hydration (20), and ischemic preconditioning (21). Epithelial and endothelial barrier function is another protective response regu-

lated by CD73-generated adenosine (22–25). Adenosine is found to be elevated in the extracellular space of tumors (16, 26) and similar responses, especially angiogenesis (27–29) and immunosuppression (3–8), are induced, leading to tumor progression. CD73 is expressed by many cell types in the tumor microenvironment, including endothelial cells and subtypes of lymphocytes and stromal cells (30), all of which contribute to CD73-mediated tumor progression (5–7).

Contrary to other tumors, such as breast and pancreatic carcinomas, which are usually fibrotic and rich in stromal cells and inflammatory components, endometrial carcinomas typically grow microscopically as interconnected malignant glands with fewer intervening stromal or inflammatory cells (31). Here, we report that CD73 downregulation in endometrial carcinoma occurs specifically in neoplastic epithelial cells. Inducing epithelial barrier function, which involves increasing cell-cell adhesions, seemingly would not be beneficial to tumors. What controls adenosine-induced tissue responses in the tumor microenvironment is currently unknown. Thus, we hypothesized that CD73-generated adenosine induces a physiological reflex to protect epithelial integrity in endometrial carcinomas, making loss of CD73 crucial for tumor progression.

Elucidating the basis for CD73 loss in endometrial carcinoma led us to unravel a unique means by which CD73-generated adenosine protects epithelial integrity. This involves adenosine A₁R-mediated (A₁R-mediated) actin polymerization and extension of cell-cell filopodia. In addition to underscoring the

Conflict of interest: The authors have declared that no conflict of interest exists.

Submitted: October 27, 2014; **Accepted:** November 3, 2015.

Reference information: *J Clin Invest.* 2016;126(1):220–238. doi:10.1172/JCI79380.

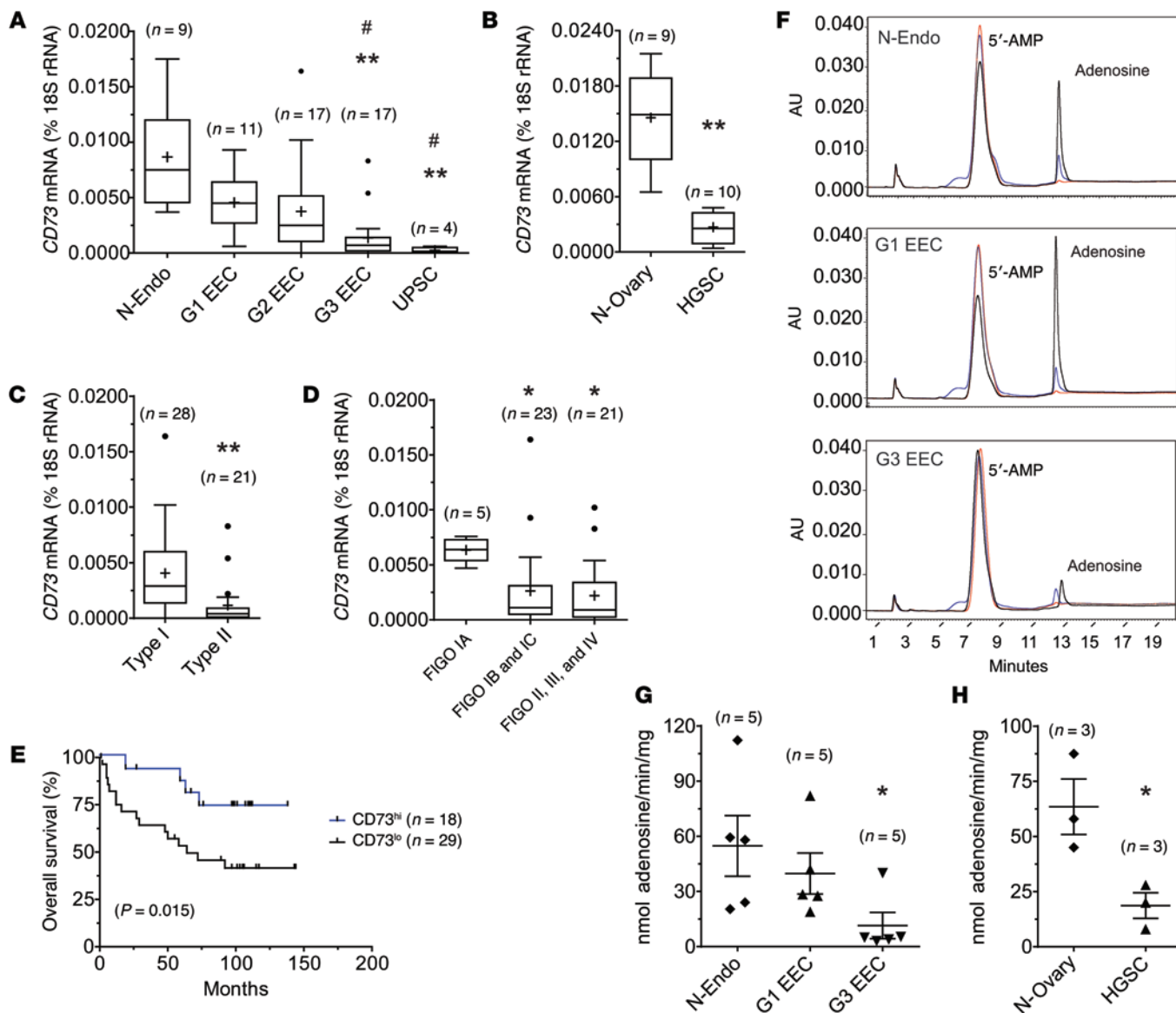


Figure 1. CD73 mRNA levels and specific activity are downregulated in high-grade, advanced-stage endometrial and ovarian carcinomas. (A, C, and D) CD73 expression by real-time qPCR in N-Endo and EECs. Data are plotted by pathologic grade (A), type I (G1 EEC and G2 EEC) and type II (G3 EEC and UPSC) classification (C), and FIGO surgical stage (D). (B) CD73 mRNA levels in N-Ovary and ovarian HGSC. Box blots represent the 25th–75th percentiles, bars represent the 50th percentile, crosses indicate the mean values, and whiskers represent the 75th percentile plus and the 25th percentile minus 1.5 times the interquartile range. Values greater than these are plotted as individual circles. (E) Kaplan-Meier curve stratified by CD73 mRNA levels. Two subjects were excluded due to death from a second cancer. (F) Representative RP-HPLC chromatograms. Red lines indicate heat-inactivated samples; blue lines indicate samples treated with the CD73 inhibitor AoPCP; black lines indicate untreated samples. (G) CD73-specific activity in N-Endo and EECs and in (H) N-Ovary and HGSC. Data represent the mean ± SEM. **P* < 0.05, ***P* < 0.001, and (A) **P* < 0.05 compared with G1 EEC. (A, D, and G) Kruskal-Wallis with Dunn's post test; (B and H) unpaired, 2-tailed *t* test; (C) Mann-Whitney *U* test; (E) Gehan-Breslow-Wilcoxon test.

complex role of CD73 in cancer, our work highlights the idea that epithelial cells are programmed to maintain cell-cell adhesions. And, like other epithelial cell components such as E-cadherin that must be downregulated for tumor progression to occur, the mediators of this important reflex must also be downregulated.

Results

CD73 is downregulated in poorly differentiated, invasive, and metastatic endometrial carcinomas. We measured the expression of CD73 in normal endometrium and endometrial carcinomas

of varying histotypes (endometrioid and nonendometrioid), tumor grade, and surgical stage. We detected no significant differences in CD73 mRNA levels between normal endometrium (N-Endo) and grade-1 endometrial endometrioid carcinomas (G1 EECs) (Figure 1A), which are well-differentiated tumors that rarely metastasize. Compared with CD73 mRNA levels in N-Endo, the levels were significantly lower in G3 EECs and nonendometrioid uterine papillary serous carcinomas (UPSCs), both of which are poorly differentiated, high-grade tumors that are associated with deep myometrial invasion and

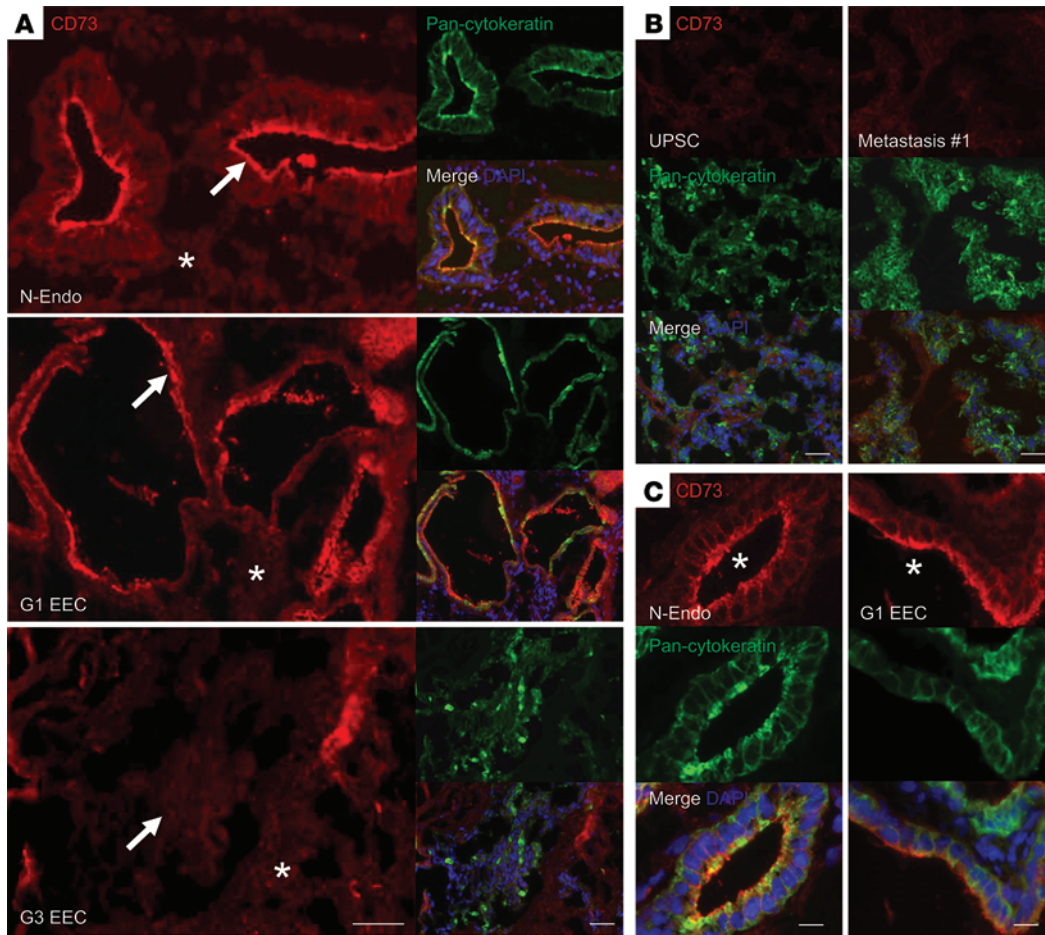


Figure 2. CD73 loss occurs in the carcinoma cells of poorly differentiated endometrial carcinomas and endometrial cancer metastases. (A and B) Cryosections of N-Endo (proliferative; $n = 3$), CD73 high (G1 EEC; $n = 3$), and CD73 low (G3 EEC and UPSC; $n = 3$) tissue and peritoneal endometrial carcinoma metastatic tissue (Metastasis #1; $n = 5$) labeled with anti-human CD73 and the epithelial cell marker pan-cytokeratin. Arrows indicate glandular epithelial cells (N-Endo) or carcinoma cells (G1 EEC and G3 EEC). Asterisks indicate stromal cells and/or connective tissue. (C) High-magnification images of glandular epithelial cells (N-Endo) and carcinoma cells from a G1 EEC gland. Asterisks indicate the glandular lumen. CD73 was expressed on apical and basolateral membranes. Scale bars: 50 μm (A and B), 20 μm (C).

metastasis. We found that *CD73* expression was also lower in the most common epithelial subtype of ovarian cancer — HGSC of the ovary, which microscopically resembles UPSC and has a similarly aggressive clinical course (Figure 1B and ref. 32). We evaluated *CD73* expression in relation to type I and type II classifications and surgical stage. Type II carcinomas are more clinically aggressive compared with type I carcinomas. We found that *CD73* expression levels were significantly lower in type II tumors (Figure 1C) and in endometrial carcinomas associated with myometrial invasion (International Federation of Gynecology and Obstetrics [FIGO] stages IB and IC) and extrauterine disease (FIGO stages II, III, and IV) compared with levels detected in noninvasive tumors (FIGO stage IA; Figure 1D). High *CD73* expression levels were associated with prolonged overall survival ($P = 0.015$; hazard ratio, 0.3606; 95% CI, 0.1486–0.8747) (Figure 1E). We also assessed *CD73* expression in The Cancer Genome Atlas (TCGA) endometrial cancer data set ($n = 270$ EECs, $n = 53$ UPSCs; ref. 33 and Supplemental Figure 1, A and B; supplemental material available online with this article; doi:10.1172/JCI79380DS1). TCGA data are in agreement with our results; *CD73* expression levels were significantly higher in endometrioid carcinomas (especially for grades 1 and 2) compared with levels in UPSCs.

The mRNA levels of other genes important for the regulation and activity of extracellular adenosine, including adenosine deaminase (*ADA*), equilibrative nucleoside transporter 1 (*ENT1*),

the adenosine receptors A_1R , $A_{2A}R$, $A_{2B}R$, and A_3R , and the adenosine receptor effector osteopontin (*SSPI*), were also measured in the same set of endometrial carcinomas. Only *CD73* expression was consistently and significantly altered with the different prognostic factors for endometrial cancer (Supplemental Table 1). We measured *CD73*-specific activity by reverse-phase HPLC (RP-HPLC) in N-Endo and representative G1 EEC and G3 EEC (Figure 1F) and found that *CD73*-generated adenosine levels were significantly lower in G3 EEC (Figure 1G). *CD73* activity accounted for $82\% \pm 4\%$ and $79\% \pm 3\%$ of the adenosine produced in N-Endo and G1 EEC, respectively. *CD73*-generated adenosine levels were also lower in HGSC of the ovary compared with levels detected in normal ovary (N-Ovary) (Figure 1H). *CD73*-specific activity was significantly correlated with *CD73* mRNA levels in both cancer types ($P = 0.0001$, Pearson's $r = 0.8896$; Figure 1F; $P = 0.0001$, Pearson's $r = 0.8916$; Figure 1G).

CD73 loss occurs in carcinoma cells. We next sought to localize the loss of *CD73* expression in endometrial carcinomas. Cryosections of N-Endo and *CD73*^{hi} (G1 EEC) and *CD73*^{lo} (G3 and UPSC) endometrial carcinomas were labeled with anti-human *CD73* and the epithelial cell marker pan-cytokeratin. In N-Endo, we detected *CD73* in glandular epithelial cells and surrounding stromal cells, with higher expression levels seen in the epithelial cells (Figure 2A). Similarly, we detected *CD73* in the carcinoma cells and stromal cells of *CD73* high tumors (G1 EEC), with higher expression levels seen in the carcinoma cells. In contrast, *CD73* expression

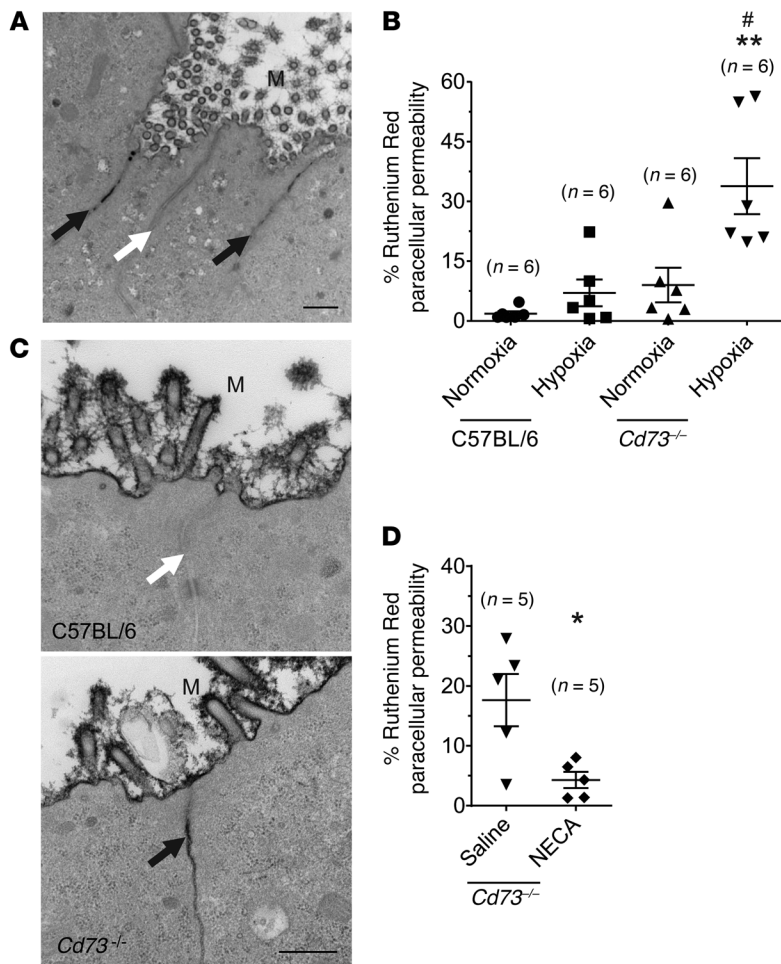


Figure 3. CD73 deficiency causes increased paracellular permeability of ruthenium red in vivo. Ten- to fourteen-week-old proestrus-staged C57BL/6 and CD73-deficient ($Cd73^{-/-}$) mice were exposed to hypoxia (7% O_2) or room air for 4 hours. Uterine horns were perfusion fixed in vivo with 0.2% ruthenium red and 2% glutaraldehyde. Ruthenium red paracellular permeability was quantified by assessing approximately 200 consecutive paracellular spaces per uterine section by transmission electron microscopy. The percentage of permeability is the ratio of paracellular spaces containing ruthenium red to the total number of paracellular spaces assessed. **(A)** Electron photomicrograph shows the presence (black arrows) and absence (white arrow) of electron-dense ruthenium red (black deposit) in the paracellular space of a uterine section. **(B)** Percentage of ruthenium red paracellular permeability for uterine sections ($n = 6$ mice). **(C)** Representative electron photomicrographs of uterine sections from C57BL/6 and $Cd73^{-/-}$ mice exposed to hypoxia (7% O_2) for 4 hours. Black arrow (bottom panel) indicates the paracellular space with ruthenium red; white arrow (top panel) indicates the paracellular space showing no ruthenium red. M, microvilli. **(D)** $Cd73^{-/-}$ mice were i.p. injected with 0.1 mg/kg NECA or DMSO prior to hypoxia exposure (7% O_2) for 4 hours. Data represent the mean \pm SEM. **(B)** $^{**}P < 0.005$ compared with hypoxic C57BL/6 mice; $^{*}P < 0.005$ compared with normoxic $Cd73^{-/-}$ mice; 1-way ANOVA with Tukey's post test. **(D)** $^{*}P = 0.019$; unpaired, 2-tailed t test. Scale bars and original magnification: **(A)** 500 nm, $\times 25,000$; **(C and D)** 500 nm, $\times 50,000$.

levels in carcinoma cells of G3 EEC and UPSC were lower compared with levels detected in G1 EEC and N-Endo glandular epithelial cells (Figure 2, A and B). CD73 was also low in carcinoma cells of metastases involving the peritoneum, omentum, and ovary (peritoneal metastasis #1, Figure 2B; omental and ovarian metastases #2-5, Supplemental Figure 2). Higher-grade endometrial carcinomas showed low expression levels of stromal CD73 that were comparable to those detected in N-Endo and G1 EEC, indicating that, although CD73 loss occurs in the carcinoma cells of tumors, stromal CD73 is not upregulated as a compensatory response. At high magnification, we observed CD73 on apical and basolateral membranes of epithelial cells of N-Endo and G1 EEC endometrial carcinoma cells (Figure 2C).

CD73 is associated with epithelial differentiation and prevents hypoxia-mediated breakdown of the epithelial barrier. Data from Figures 1 and 2 suggest that CD73 is related to epithelial differentiation in the endometrium. This finding was also supported in vitro. CD73 mRNA levels and specific activity were significantly lower in moderately and poorly differentiated endometrial carcinoma cell lines compared with those detected in the well-differentiated HEC-1-A and HEC-1-B cells (Supplemental Figure 3). We further assessed this association in Wistar Institute Susan Hayflick (WISH) cells, which spontaneously transition from a mesenchymal-like to an epithelial-like growth pattern (Supplemental Figure 4A) and differentiation state

(Supplemental Figure 4B) with increasing confluency. CD73 mRNA levels were significantly increased in WISH cells that had epithelial-like differentiation (100% and 2 Day-Post and 4 Day-Post confluency; Supplemental Figure 4C). CD73 was also localized to cells in closer proximity to each other (more epithelial-like; Supplemental Figure 4D), suggesting that CD73 is important for epithelial integrity.

CD73-generated adenosine protects tissue integrity by inducing endothelial (22-24) and intestinal epithelial (25) barrier function. Therefore, we examined the effect of CD73 deficiency on the epithelial barrier in normal endometrium. Uterine horns of CD73-deficient ($Cd73^{-/-}$) mice and C57BL/6 mice were perfused in vivo with ruthenium red, and loss of barrier function was assessed by electron microscopic examination of ruthenium red movement through the paracellular space of uterine luminal epithelial cells (Figure 3A). We found, as expected, that barrier function was comparable between $Cd73^{-/-}$ and C57BL/6 mice in normoxia; $Cd73^{-/-}$ mice generally do not show a loss in barrier function until hypoxic (Figure 3B and ref. 24). With whole-animal hypoxia (7% O_2 , 4 hours), a significant increase in ruthenium red paracellular permeability occurred in $Cd73^{-/-}$ mice compared with C57BL/6 and normoxic $Cd73^{-/-}$ mice, indicating loss of barrier function (Figure 3B). Representative electron photomicrographs of uterine sections from C57BL/6 and $Cd73^{-/-}$ mice exposed to hypoxic conditions are shown in Figure 3C.

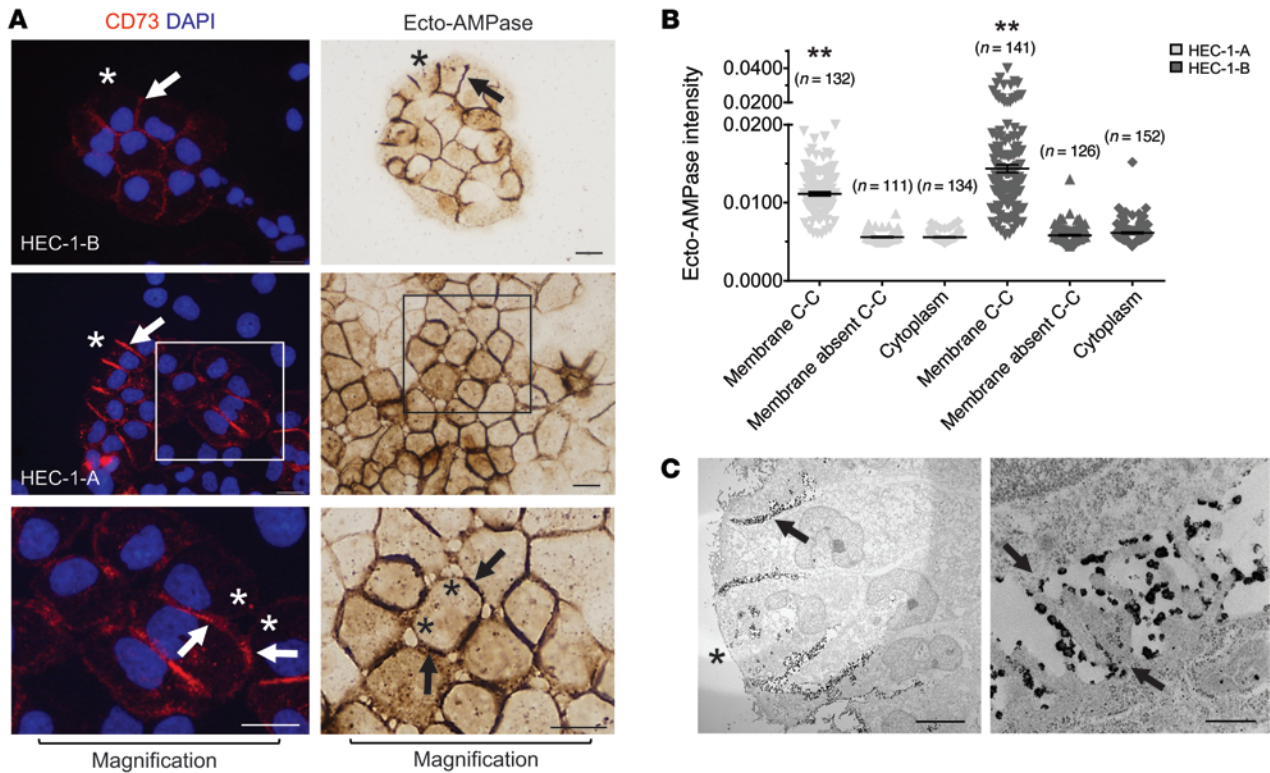


Figure 4. CD73 localizes to membrane areas of cell-cell contacts and filopodia. (A) CD73 immunofluorescence and ecto-AMPase activity (brown deposit), in the presence of 5 mM levamisole, in HEC-1-A cells. Asterisks indicate membrane areas absent of cell-cell contact; arrows indicate membrane areas of cell-cell contact. (B) Ecto-AMPase intensity by regions of interest (ROIs) placed at membrane areas of cell-cell contact, membrane areas absent of cell-to-cell contact, and in the cytoplasm (ImageJ software; NIH). ROI intensity was corrected by inverting the mean (1/ROI mean intensity). ROIs were assessed in 10 images at $\times 40$ original magnification for 10 to 25 cells per image. Total ROIs are indicated as (n =). Data are expressed as the mean \pm SEM. $^{***}P < 0.001$; 1-way ANOVA with Tukey's post test. C-C, cell-to-cell contact. (C) Electron photomicrographs of ecto-AMPase activity (black deposit) in HEC-1-A cells. Left panel: low-magnification image of cell-cell contacts showing ecto-AMPase activity. Right panel: high-magnification image of a cell-cell contact with ecto-AMPase activity and filopodia (arrows). Scale bars and original magnification: 20 μ m (A), 10 μ m, $\times 2,500$ (C, left panel); 500 nm, $\times 50,000$ (C, right panel).

5'-N-ethylcarboxamidoadenosine (NECA) is a stable adenosine analog that exhibits mixed agonist properties for the adenosine receptors. NECA, injected i.p. prior to whole-animal hypoxia, reduced ruthenium red permeability in *Cd73*^{-/-} mice (Figure 3D), indicating that CD73-generated adenosine protects barrier function in endometrial epithelial cells.

CD73 localizes specifically to cell-cell contacts and associates with cell-cell filopodia. HEC-1-A and HEC-1-B cell lines were derived from a FIGO IA endometrial tumor (Figure 1D and ref. 34) and showed high *CD73* mRNA levels and specific activity (Supplemental Figure 3, B and C, respectively). Interestingly, we observed that CD73 localized specifically to membrane areas of cell-cell contacts (Figure 4A). This is uncharacteristic of CD73, as membrane localization of GPI-anchored proteins is generally independent of cell-cell contact (35). Localization of CD73 did not change when cells were grown on collagen-coated coverslips (data not shown). Similarly, we found that ecto-AMPase activity (an indicator of CD73 activity) was localized to membrane areas of cell-cell contact in subconfluent and confluent cells (Figure 4A, right panels). Ecto-AMPase intensity at membrane areas of cell-cell contact and those absent of cell-cell contact are shown in Figure 4B. Membrane areas of cell-cell contacts were examined ultrastructurally and showed extensive cell-cell filopodia with ecto-AMPase activity (Figure 4C, right panel).

Specific proteins often associate with filopodia on the basis of function. For example, E-cadherin localizes with cell-cell filopodia and β_1 integrins with focal adhesion filopodia (36, 37). We questioned whether CD73 expression was specific to cell-cell filopodia. Both filopodia of focal adhesions and cell-cell contacts are short-length filopodia. E-cadherin (Supplemental Figure 5, A and B; HEC-1-B cells did not express E-cadherin, data not shown) and CD73 (Figure 5, A and B) localized only with the filopodia of cell-cell contacts in HEC-1-A cells and were both absent from the filopodia of focal adhesions.

In mammalian epithelial cells (38, 39), *Caenorhabditis elegans* (40, 41), and *Drosophila melanogaster* (42–44), cell-cell filopodia are central to forming intercellular adhesions. Filopodia from opposing cells interdigitate progressively down the length of the membrane, aligning the two membranes and establishing initial, then mature, intercellular adhesions (45). These structures are known as membrane zippers (39). Both HEC-1-A and HEC-1-B cells showed apparent membrane zippers with ecto-AMPase activity (HEC-1-B cells, Figure 5C; HEC-1-A cells, Supplemental Figure 6). Long- and short-length cell-cell filopodia are shown in Figure 5C; however, high ecto-AMPase activity occurred only with short-length filopodia (approximately ≤ 3 μ m in length; Figure 5C, accompanying

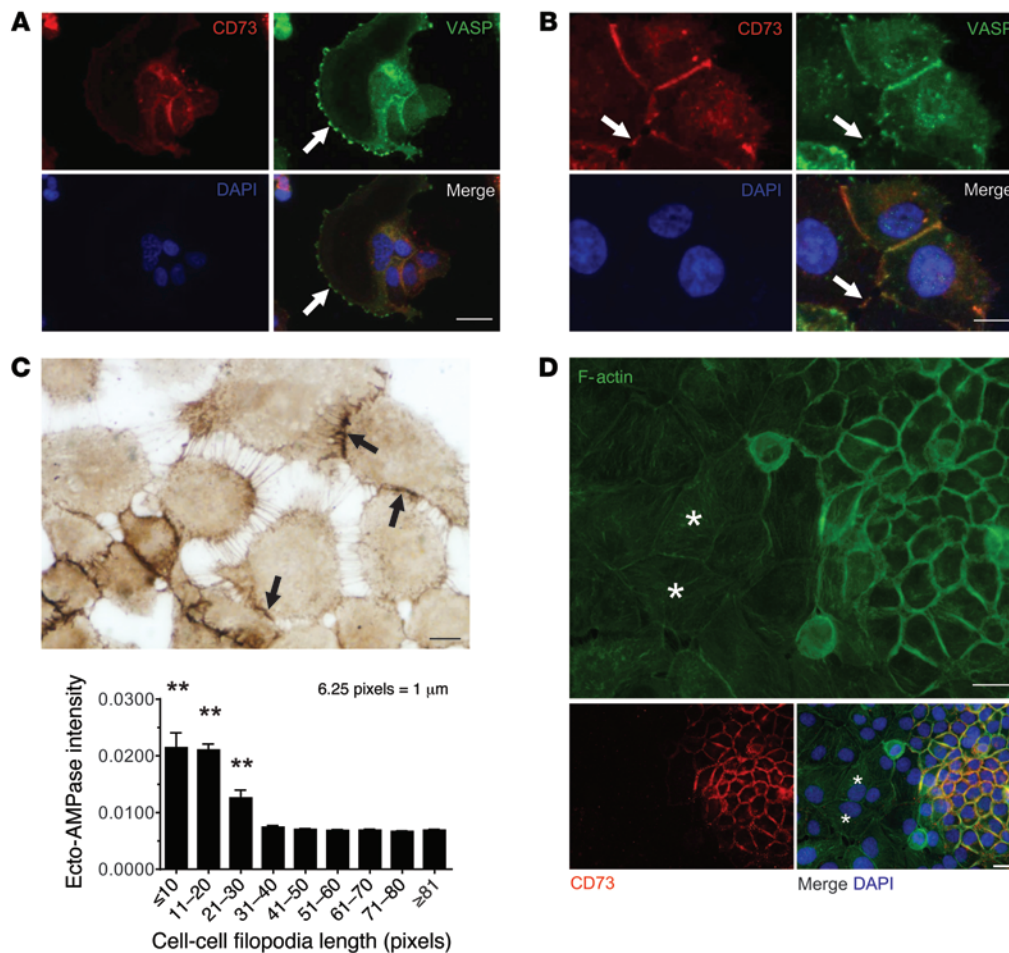


Figure 5. CD73 associates with filopodia of cell-cell contacts and circumferential cortical F-actin. CD73 is absent from the filopodia of focal adhesions (A) and is expressed with the filopodia of cell-cell contacts (B) in HEC-1-A cells. VASP is a nonspecific marker of filopodia (arrows). (C) Ecto-AMPase activity (brown deposit) associates with membrane zippers (arrows), filopodia-dense structures involved in forming intercellular adhesions, in HEC-1-B cells. Graph shows ecto-AMPase intensity at membrane areas with filopodia of different lengths. Ecto-AMPase intensity was assessed in 40 images at $\times 40$ original magnification using ROIs placed at membrane areas of cells with filopodia. ROI intensity (ImageJ software) and the length of the corresponding filopodia (pixels) (Olympus cellSens Dimension software) were measured and ranged from 23 ROIs to 128 ROIs (see Supplemental Methods). ROI intensity was corrected by inverting the mean ($1/\text{ROI mean intensity}$). Data are expressed as the mean \pm SEM. $^{**}P < 0.001$; 1-way ANOVA with Tukey's post test. (D) HEC-1-A cells labeled with anti-human CD73 and Alexa Fluor-conjugated phalloidin (F-actin). CD73 was absent in cells with minimal circumferential cortical F-actin (asterisks). Scale bars: 50 μm (A), 20 μm (B and D), 100 pixels or 16 μm (C).

graph), which are filopodia indicative of intercellular adhesions. Collectively, these associations suggest that CD73-generated adenosine regulates cell-cell adhesions.

CD73-generated adenosine regulates membrane filamentous actin. Given that filamentous actin (F-actin) is the primary component of filopodia and membrane zippers are dependent on actin polymerization (39), we hypothesized that CD73-generated adenosine regulates cell-cell adhesions by regulating F-actin. We observed a strong association between CD73 and circumferential cortical F-actin (Figure 5D, HEC-1-A cells, $P < 0.001$, Pearson's $r = 0.7081$; Supplemental Figure 7A, HEC-1-B cells, $P < 0.001$, Pearson's $r = 0.7198$). Importantly, we found that cells merely in contact with each other, without sufficient cortical F-actin, were not associated with CD73 (see cells with asterisks in Figure 5D and HEC-1-B cells in Supplemental Figure 7, B-D). Changes in F-actin were assessed by isolating total actin from confluent HEC-1-A cells exposed to hypoxia (1% O_2 , 5% CO_2) for 36 hours

and treated with the CD73 inhibitor AoPCP for 50 minutes. Hypoxia was used as a tumor-relevant stressor (46). Inhibition of CD73 resulted in a 43%–54% decrease in total F-actin (Figure 6A). This decrease in F-actin was accompanied by an increase in globular actin (G-actin), which was expected, given the short duration (50 minutes) between treatment time and actin isolation. The G-actin/F-actin ratio (non-normalized data; samples individually assessed for parallel F-actin decrease/G-actin increase) for untreated HEC-1-A cells and HEC-1-A cells treated with 5'-AMP, 5'-AMP plus AoPCP no. 1, or 5'-AMP plus AoPCP no. 2 is shown in Figure 6B. Phalloidin staining showed that F-actin was primarily at the membrane of untreated and 5'-AMP-treated HEC-1-A cells (Figure 6C). AoPCP-treated cells, however, showed a 42% decrease in cortical F-actin (Figure 6, C and D). This was similar to the decrease in F-actin levels observed by isolating total actin, indicating that the regulation of F-actin by CD73-generated adenosine is, in large part, specific to cortical actin.

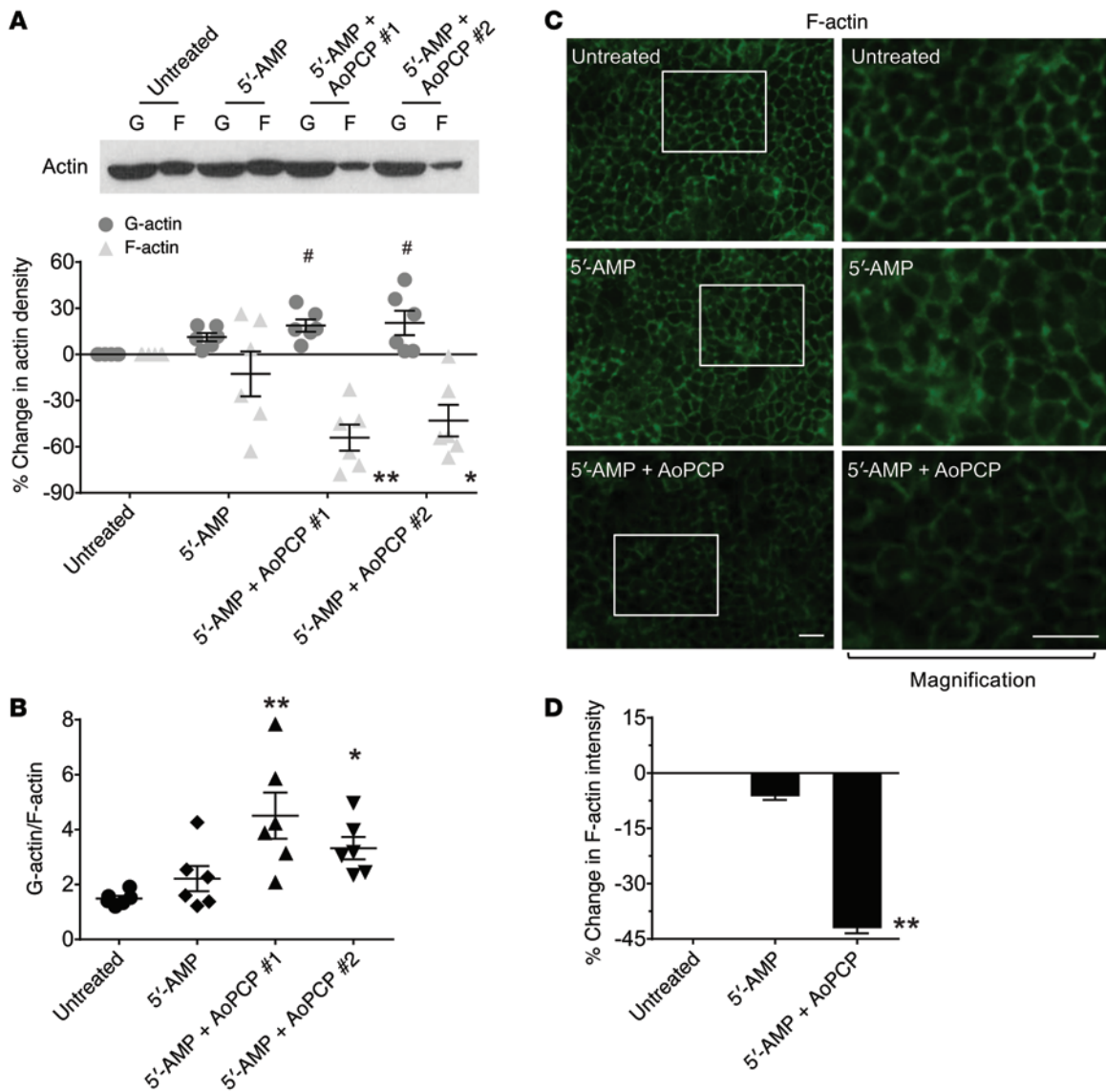


Figure 6. The CD73 inhibitor AoPCP decreases circumferential cortical F-actin. (A) Representative immunoblot of total actin (G- and F-actin) isolated from confluent HEC-1-A cells untreated (control) or treated with 50 μ M 5'-AMP or 50 μ M 5'-AMP plus 100 μ M AoPCP for 50 minutes following 36 hours of hypoxia (1% O₂, 5% CO₂). DCF (10 μ M) was included with treatments and controls. HEC-1-A cells were pretreated with 100 μ M AoPCP or fresh Opti-MEM for 1 hour. 5'-AMP plus AoPCP no. 1 and 5'-AMP plus AoPCP no. 2 were independent replicates in a single experiment. Graph shows densitometric data from 6 independent experiments; 1 experiment ($n = 7$) was excluded because of values that exceeded ± 2 SD. ** $P < 0.005$, * $P < 0.05$, and # $P < 0.05$; 1-way ANOVA with Tukey's post test. 5'-AMP and AoPCP dose responses are shown in Supplemental Figures 8 and 9. (B) G-actin/F-actin ratio. *** $P < 0.005$ and * $P < 0.05$; 1-way ANOVA with Holm-Sidak post test. (C) Alexa Fluor-conjugated phalloidin immunofluorescence in HEC-1-A cells. Cortical F-actin decreased with AoPCP. Scale bars: 20 μ m. (D) F-actin intensity was assessed in at least 10 or more images (original magnification, $\times 20$) using cellSens Dimension software, set at "Automatic Threshold." *** $P < 0.001$; 1-way ANOVA with Tukey's post test. All data are expressed as the mean \pm SEM.

To examine whether increasing CD73 increases F-actin, we first examined whether CD73 is induced by hypoxia in endometrial carcinoma cells. Hypoxia-inducible factor 1 α (HIF-1 α) induces CD73 and A_{2B}R expression in models of barrier function (25, 47). Contrary to our expectations, CD73 was not induced in HEC-1-A or HEC-1-B cells, but A_{2B}R was induced (Supplemental Figure 10). Therefore, we treated HEC-1-A cells with increasing concentrations of human recombinant CD73 for 50 minutes. Total actin was isolated from confluent HEC-1-A cells and exposed to hypoxia (1% O₂, 5% CO₂) for 36 hours. Total F-actin increased by 23% with 100 ng/ml recombinant CD73 (Fig-

ure 7A), accompanied by a significant decrease in G-actin. We observed similar F-actin increases of 20% and 16% with 1 ng/ml and 10 ng/ml recombinant CD73 treatment, respectively, but these increases did not reach significance ($P = 0.054$, 1 ng/ml; $P = 0.144$, 10 ng/ml). The non-normalized data, expressed as a G-actin/F-actin ratio, are shown in Figure 7B. Phalloidin staining showed a 27% increase in cortical F-actin with 100 ng/ml human recombinant CD73 treatment (Figure 7C, accompanying graph). We observed similar results in HEC-1-A cells treated with 5'-nucleotidase from *Crotalus atrox* venom (Supplemental Figure 11). Total F-actin increased by 47% after treatment with

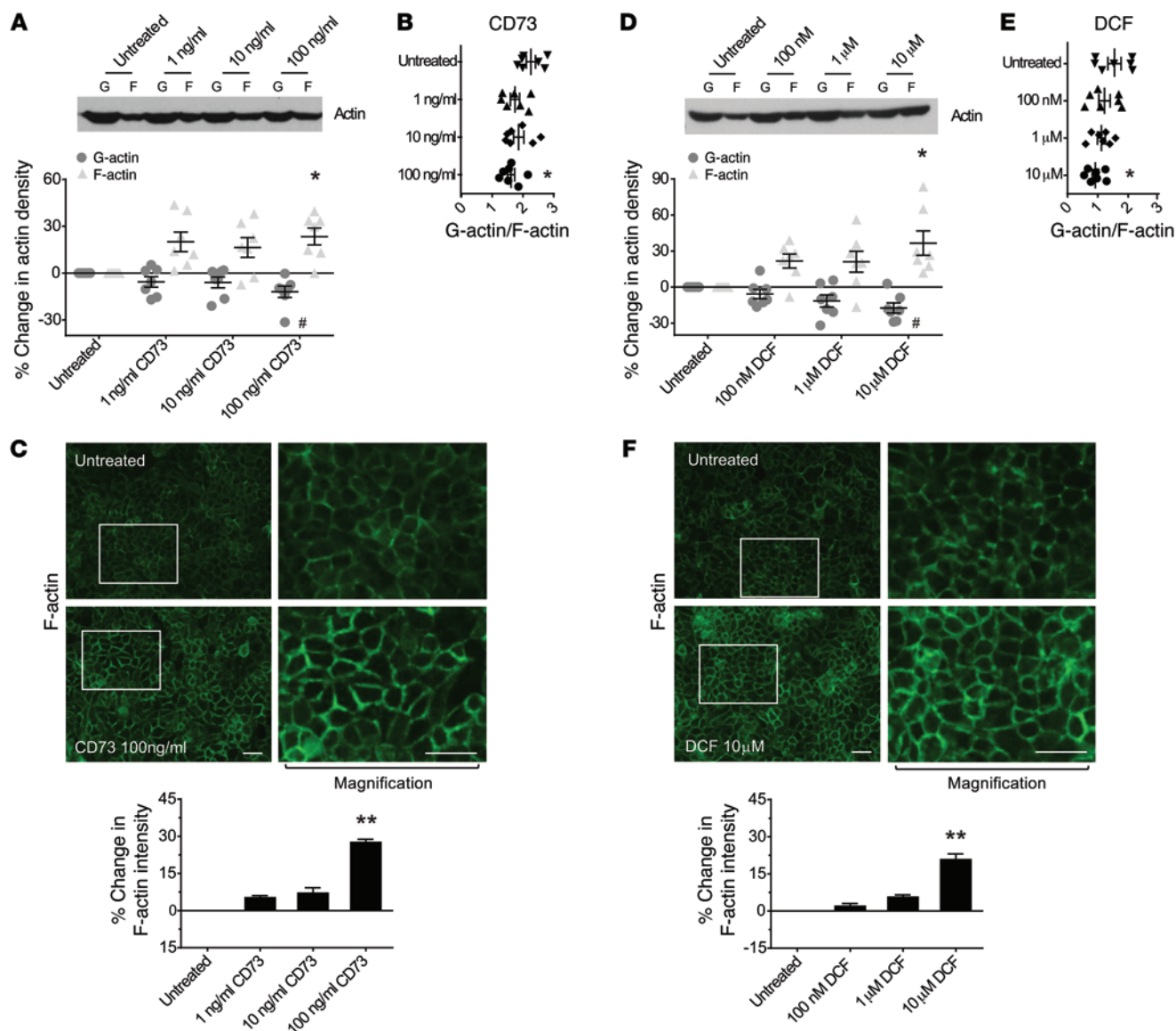


Figure 7. CD73-generated adenosine induces cortical F-actin. (A and D) Representative immunoblots of total actin isolated from confluent HEC-1-A cells. (A) HEC-1-A cells treated with 50 μ M 5'-AMP (untreated) or 50 μ M 5'-AMP plus human recombinant CD73 for 50 minutes following 36 hours of hypoxia (1% O_2 , 5% CO_2). DCF (10 μ M) was included with treatments and controls (untreated). (D) HEC-1-A cells treated with 50 μ M 5'-AMP plus DMSO (untreated) or 50 μ M 5'-AMP plus DCF. Graphs in A and D show the densitometric data from 7 independent experiments each. (B and E) G-actin/F-actin ratios. (C and F) Alexa Fluor-conjugated phalloidin staining (F-actin) in HEC-1-A cells treated with human recombinant CD73 (C) or DCF (F). Scale bars: 20 μ m. Graphs show F-actin intensity as assessed in 15 or more images (original magnification, $\times 20$) using cellSens Dimension software, Adaptive Threshold. Data are expressed as the mean \pm SEM. * P < 0.05 for F-actin and # P < 0.05 for G-actin compared with untreated cells, by 1-way ANOVA with Tukey's post test (A and D) and by Holm-Sidak post test (B and E). ** P < 0.001 for F-actin intensity, by 1-way ANOVA with Tukey's post test (C and F).

0.01 U *Crotalus atrox* 5'-nucleotidase, and phalloidin staining showed a significant increase in F-actin at the membrane (21%; P < 0.001). We found that G-actin levels decreased as well. The G-actin/F-actin ratios were as follows: 1.92 ± 0.19 for untreated HEC-1-A cells and 1.70 ± 0.14 for HEC-1-A cells treated with 0.001 U *Crotalus atrox* 5'-nucleotidase, 1.50 ± 0.10 with 0.005 U, and 1.14 ± 0.12 with 0.01 U.

To assess whether increasing extracellular adenosine would increase F-actin levels, we treated confluent HEC-1-A cells exposed to hypoxia (1% O_2 , 5% CO_2) for 36 hours with increasing concentrations of the adenosine deaminase inhibi-

tor 2'-deoxycoformycin (DCF) for 50 minutes. We found that treatment with DCF (10 μ M) increased total F-actin levels by 37% (Figure 7D) and was accompanied by a decrease in G-actin levels. Similar to what we observed with lower concentrations of recombinant CD73, lower concentrations of DCF (100 nM and 1 μ M) resulted in a statistically insignificant 20% decrease in total F-actin levels. The ratios of G-actin/F-actin are shown in Figure 7E. Phalloidin staining showed a 21% increase in cortical F-actin with 10 μ M DCF treatment (Figure 7F). Together, these data suggest that CD73-generated adenosine induces cortical F-actin polymerization.

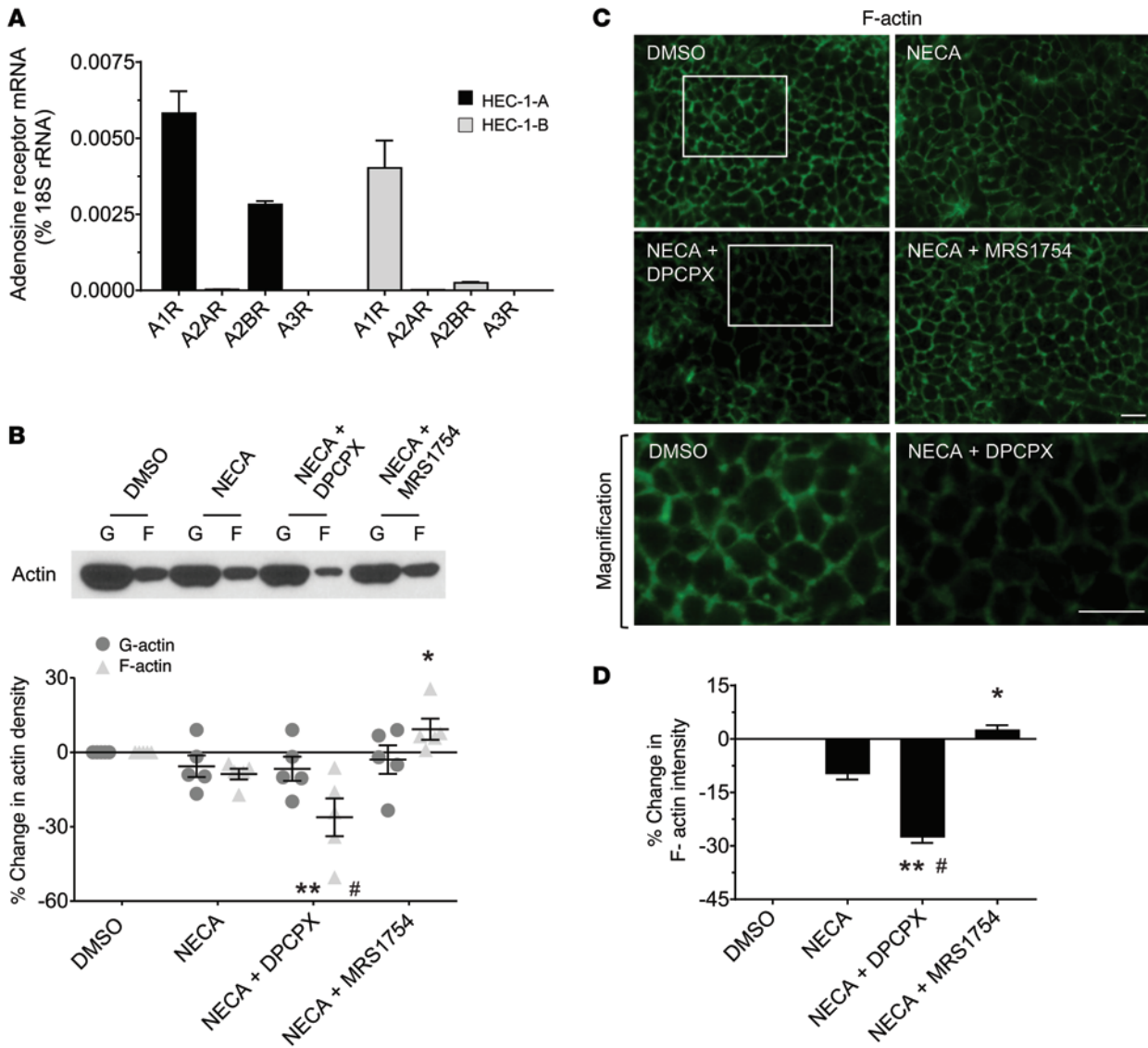


Figure 8. The adenosine A₁R antagonist DPCPX decreases cortical F-actin. (A) Adenosine receptor mRNA expression by real-time qPCR. (B) Representative immunoblot of total actin isolated from confluent HEC-1-A cells treated with DMSO (0.001%), 10 μM NECA, 10 μM NECA plus the A₁R antagonist DPCPX (10 μM) or plus the A_{2B}R antagonist MRS1754 (10 μM) in hypoxia (1% O₂, 5% CO₂) for 36 hours. Graph shows densitometric data from 5 independent experiments. (C) HEC-1-A cells labeled with Alexa Fluor-conjugated phalloidin. (D) F-actin intensity was assessed in 10 or more images (original magnification, ×20). Data represent the mean ± SEM. ***P* < 0.005 compared with DMSO; **P* < 0.05 compared with NECA; and #*P* < 0.001 compared with NECA plus MRS1754; 1-way ANOVA with Tukey’s post test. Scale bars: 20 μm.

Regulation of cortical F-actin involves the adenosine A₁ receptor. Many of the tissue-protective events attributed to CD73 occur through one or more of four G protein-coupled adenosine receptors: A₁R, A_{2A}R, A_{2B}R, and A₃R (48). We sought to determine whether CD73 regulated F-actin via an adenosine receptor. HEC-1-A and HEC-1-B cells expressed A₁R and A_{2B}R, with A₁R levels being the highest (Figure 8A). A_{2A}R and A₃R were essentially undetectable. We found that A₁R was highly expressed by most endometrial carcinoma cell lines. In contrast, breast carcinoma cell lines highly expressed A_{2B}R (Supplemental Figure 12). Total F-actin levels did not significantly change in HEC-1-A cells treated with NECA. However, NECA plus the A₁R antagonist DPCPX decreased F-actin levels by 26% (Figure 8B). NECA plus the A_{2B}R antagonist MRS1754 increased total F-actin levels by approximately 19% compared with

NECA alone, suggesting that A_{2B}R may negatively regulate the induction of F-actin by the A₁R. G-actin levels are known to normalize with time (49); accordingly, we found that G-actin levels did not change, given the length of time between treatment and actin isolation (36 hours, Figure 8B). Cell viability was unaltered with NECA or NECA plus adenosine receptor antagonists (Supplemental Figure 13). F-actin, regardless of treatment, was mainly seen at the membrane (Figure 8C). However, in HEC-1-A cells treated with NECA plus DPCPX, we observed a significant (33%) decrease in cortical F-actin (Figure 8, C and D). These data indicate that the regulation of cortical F-actin by CD73-generated adenosine occurs via A₁R.

Cell-cell filopodia are shortened by adenosine A₁R antagonism. Next, we examined whether the regulation of cortical F-actin by A₁R also involves cell-cell filopodia. Confluent HEC-1-A cells

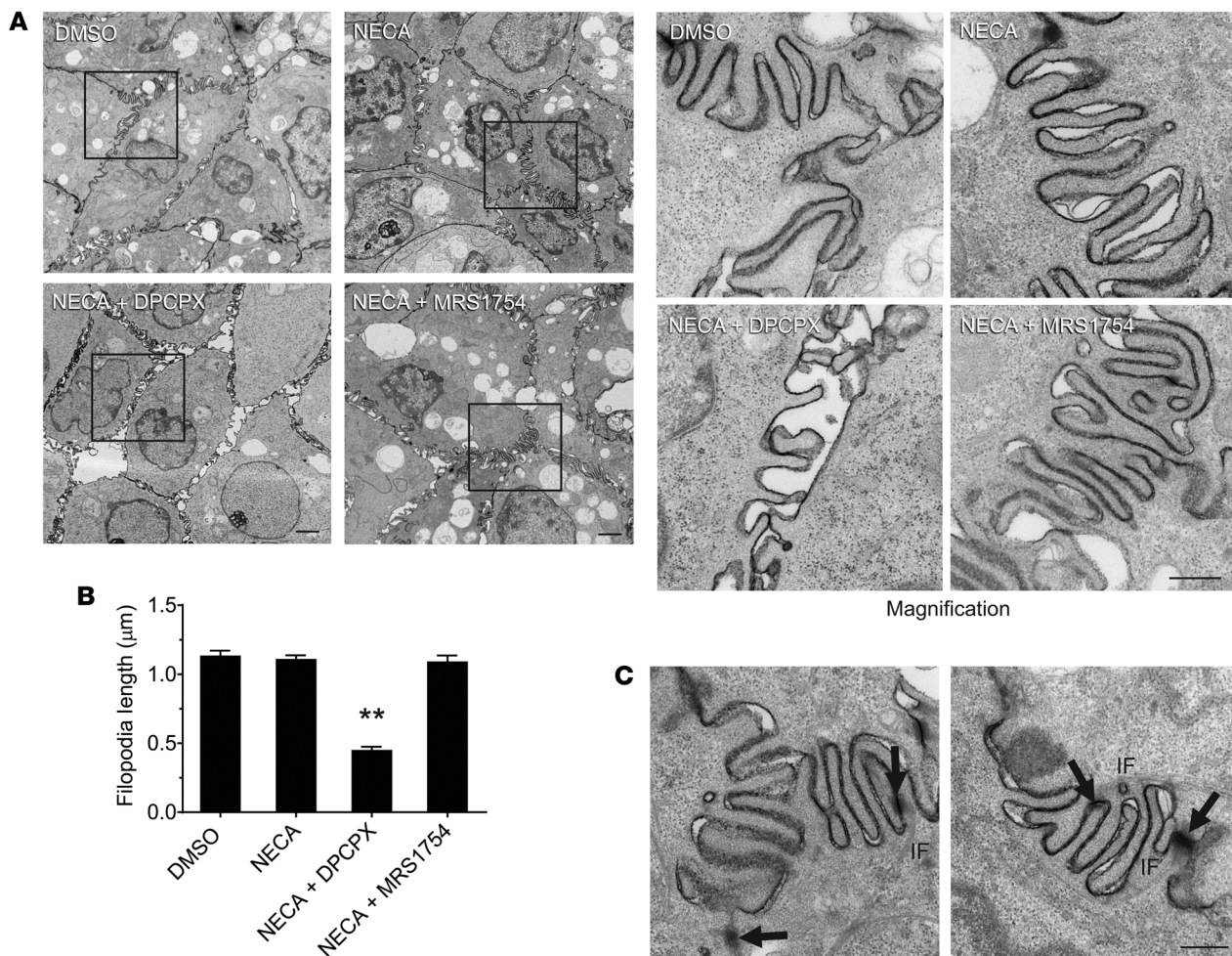


Figure 9. Adenosine A_1R antagonism shortens cell-cell filopodia length. (A) Representative electron photomicrographs. Confluent HEC-1-A cells treated with DMSO (0.001%), 10 μ M NECA, 1 μ M NECA plus the A_1R antagonist DPCPX (1 μ M) or plus the $A_{2b}R$ antagonist MRS1754 (1 μ M) in hypoxia (1% O_2 , 5% CO_2) for 36 hours. HEC-1-A cell membrane borders were enhanced with ruthenium red staining (black deposit) after 36 hours of hypoxia. (B) Filopodia lengths were measured from printed electron photomicrographs, with the print magnification calculated as $\times 8.5$ (print scale bar measurement/actual scale bar measurement). The actual length of individual filopodia was calculated by dividing by the print magnification. More than 150 filopodia from 10 or more electron photomicrographs taken from 3 replicates per treatment were measured. (C) Electron photomicrographs show desmosomes bordering areas of interdigitating filopodia (arrows). IF, intermediate filaments. Data represent the mean \pm SEM. ** $P < 0.001$; 1-way ANOVA with Tukey's post test. Scale bars and original magnification: (A) 2 μ m, $\times 5,000$ (higher-magnification images in right panels) and (C) 500 nm, $\times 50,000$.

were exposed to hypoxia (1% O_2 , 5% CO_2) for 36 hours and then assessed ultrastructurally. Cell-cell filopodia were identified in all of the groups (Figure 9A) but were significantly shorter in HEC-1-A cells treated with the A_1R antagonist DPCPX (Figure 9, A and B). We found that filopodia in DMSO-, NECA-, and NECA plus MRS1754-treated cells were completely embedded into the opposing cell and were approximately $1.08\text{--}1.13 \mu\text{m} \pm 0.02\text{--}0.04 \mu\text{m}$ in length. In primary keratinocytes, filopodia embed into the membrane at a comparable depth of approximately $1.1 \mu\text{m} \pm 0.2 \mu\text{m}$ (39). This depth coincides with the positioning of circumferential cortical F-actin (adhesion belt) and E-cadherin-catenin complexes seen by immunofluorescence, alluding to the formation of intercellular adhesions (39, 45). Notably, we observed desmosomes bordering the sites of the interdigitating filopodia (Figure 9C). Desmosomes flanking interdigitating filopodia are also seen in primary keratinocytes (39). Considering that desmosome assembly is dependent on the preceding assembly

of adherens junctions (50), it is likely that HEC-1-A cells are engaged with re-forming intercellular adhesions. Additionally, these data show that well-differentiated endometrial carcinoma cells have an intact capacity to generate adenosine and respond to its signaling to induce a physiological reflex, typical of non-neoplastic epithelial cells, to re-form cell-cell adhesions in response to hypoxia.

A_1R induces actin polymerization and involves *Cdc42* and *N-WASP*. We next sought to determine whether the regulation of cortical F-actin by A_1R is due to A_1R -mediated actin polymerization. Confluent HEC-1-A cells were exposed to hypoxia (1% O_2 , 5% CO_2) for 36 hours and treated with the A_1R agonist *N*(6)-cyclopentyladenosine (CPA). Significant total F-actin increases of 30% and 28% were seen after treatment with 1 μ M and 10 μ M CPA, respectively (Figure 10A), and no alteration in cell viability was observed (Supplemental Figure 14). Phalloidin staining showed that the change in F-actin was primarily at the membrane (Figure 10B).

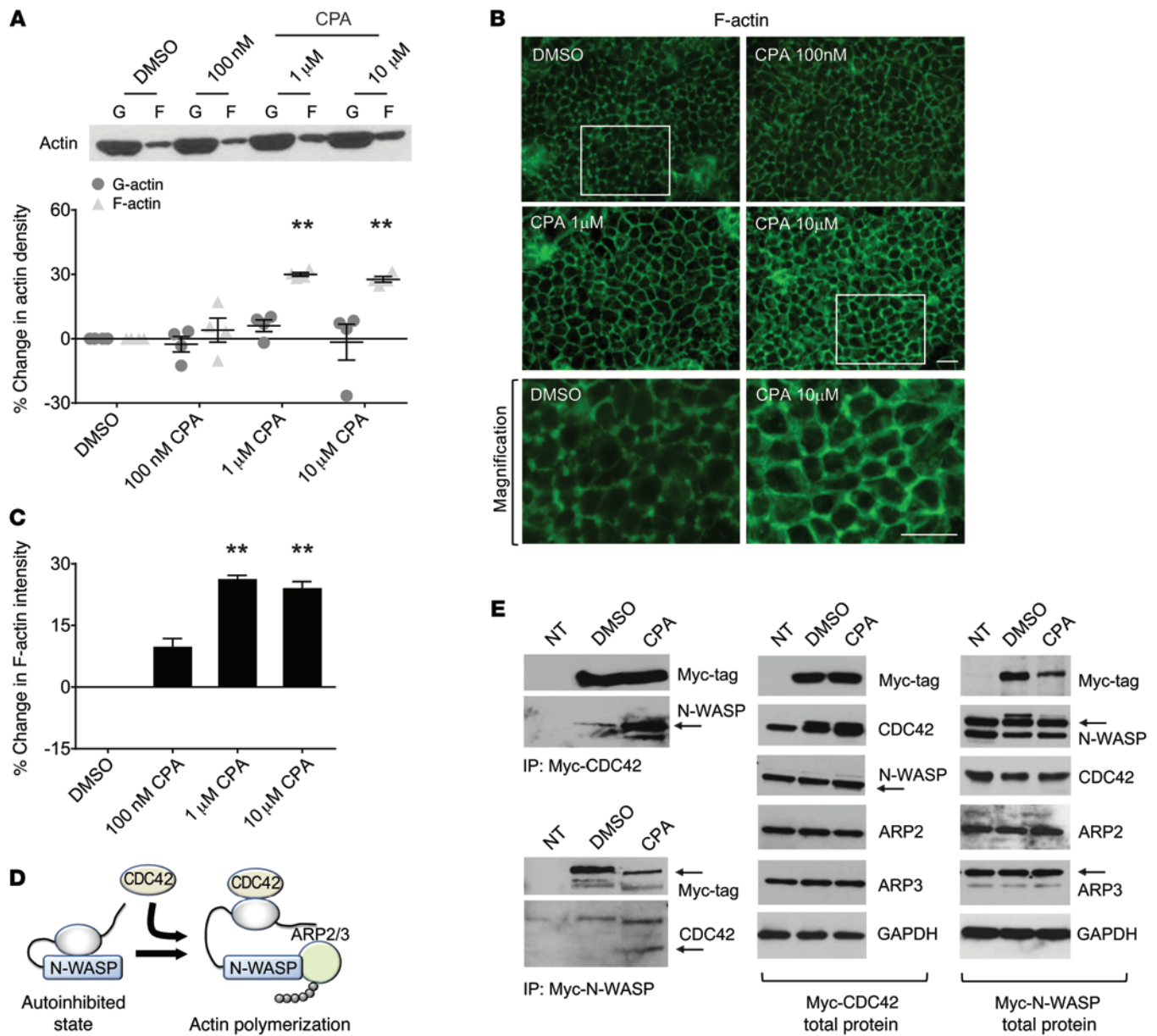


Figure 10. Adenosine A₁R induces actin polymerization. (A) Representative immunoblot of total actin isolated from confluent HEC-1-A cells treated with DMSO (0.001%) or 100 nM, 1 μM, or 10 μM of the A₁R agonist CPA in hypoxia (1% O₂, 5% CO₂) for 36 hours. Graph shows densitometric data for 4 independent experiments. (B) Alexa Fluor-conjugated phalloidin in DMSO- and CPA-treated HEC-1-A cells. Scale bars: 20 μm. (C) F-actin intensity was assessed in 10 or more images (original magnification, ×20). (D) Schematic of Rho GTPase CDC42 and the ARP2/3 actin polymerization complex member N-WASP. CDC42 binds to N-WASP, releasing its autoinhibited state. (E) Co-IP. HEC-1-A cells (90% confluent) were transfected with 2 μg Myc-tagged CDC42 or 2 μg Myc-tagged N-WASP 24 hours before hypoxia and then treated with DMSO (0.001%) or 10 μM CPA in hypoxia (1% O₂, 5% CO₂) for 36 hours. Co-IP immunoblots are representative of 3 (Myc-CDC42) and 2 (Myc-N-WASP) independent experiments (for experimental replicates, see Supplemental Figure 15). NT, nontransfected. Data represent the mean ± SEM. **P < 0.001; 1-way ANOVA with Tukey's post test.

Cortical F-actin intensity significantly increased with 1 μM CPA (26%) and 10 μM CPA (24%) treatment (Figure 10C).

The Rho GTPase family member CDC42 and neural Wiskott-Aldrich syndrome protein (N-WASP), a ubiquitously expressed CDC42-interacting protein, are important mediators of actin polymerization in mammalian cells (51), and both are implicated in filopodia formation (52–54). N-WASP is normally held in an autoinhibitory conformation. Actin polymerization occurs via binding of CDC42 to N-WASP, releasing its autoin-

hibition and thereby allowing for the binding of actin-related proteins 2 and 3 (ARP2/3) (Figure 10D and ref. 51). In HEC-1-A cells treated with 10 μM CPA, N-WASP was coimmunoprecipitated by CDC42 (Figure 10E, top left panel), and CDC42 was coimmunoprecipitated by N-WASP (Figure 10E, bottom left panel), indicating that A₁R induces actin polymerization involving the ARP2/3 actin polymerization complex.

Intercellular adhesion proteins increase at the membrane with the A₁R agonist CPA. Given that CPA increased cortical F-actin, we

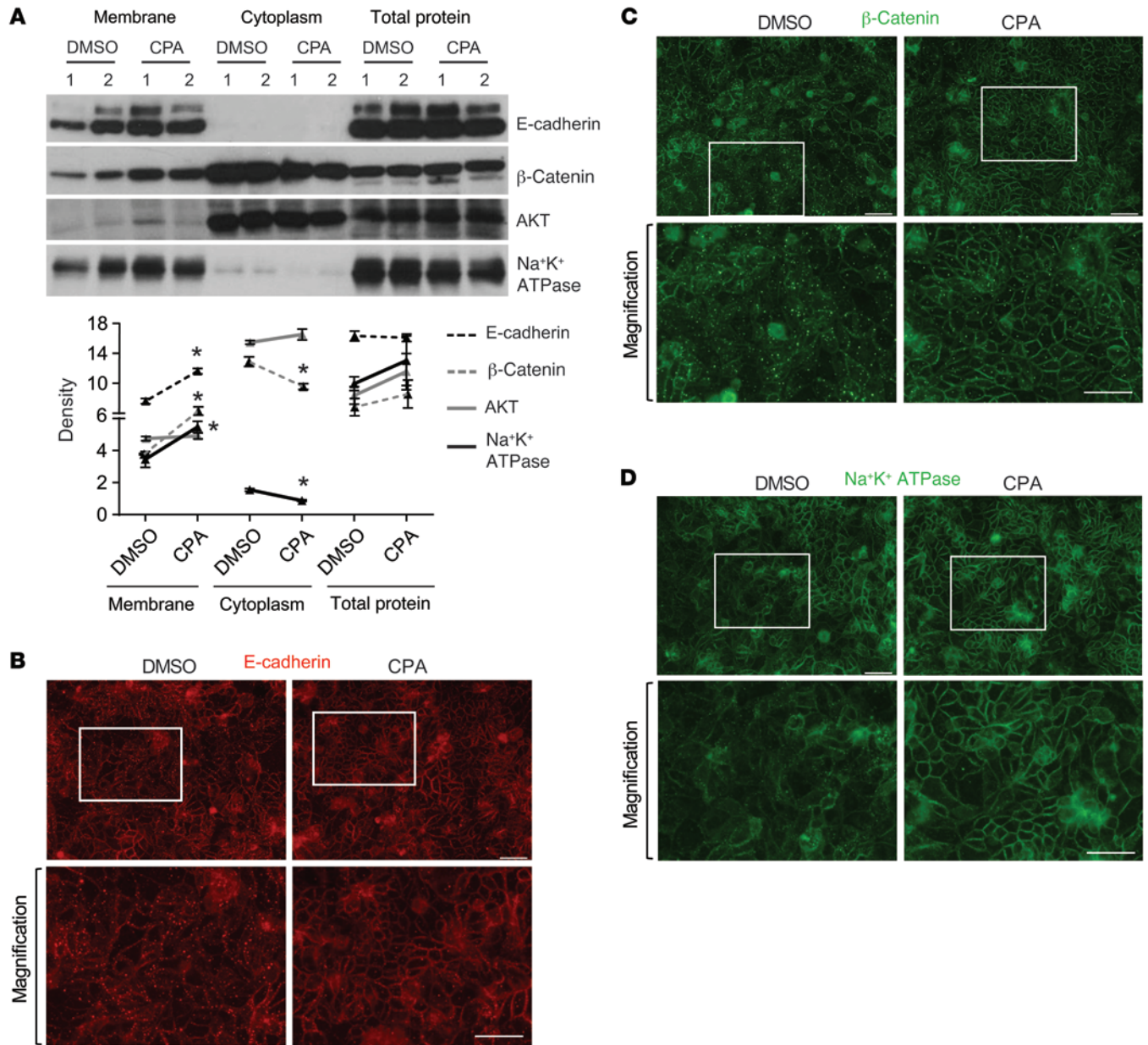


Figure 11. CPA increases membrane localization of E-cadherin, β-catenin, and Na⁺K⁺ ATPase. (A) Representative immunoblots of cellular fractions from confluent HEC-1-A cells treated with DMSO (0.001%) or 10 μM CPA in hypoxia (1% O₂, 5% CO₂) for 36 hours. Graph shows densitometric data from 2 independent experiments. DMSO no. 1 and DMSO no. 2 and CPA no. 1 and CPA no. 2 represent independent replicates in a single experiment. Data are expressed as the mean ± SEM. *P < 0.05; unpaired 2-tailed t test. AKT confirmed the purity of membrane fractions. (B–D) E-cadherin, β-catenin, and Na⁺K⁺ ATPase immunofluorescence showed increased membrane expression in HEC-1-A cells treated with 10 μM CPA in hypoxia (1% O₂, 5% CO₂) for 36 hours. Scale bars: 20 μm.

considered that an increase in intercellular adhesions would follow. We found that E-cadherin, β-catenin, and Na⁺K⁺ ATPase were increased in membrane fractions of HEC-1-A cells treated with 10 μM CPA (Figure 11A). Cytoplasmic fractions showed decreased β-catenin and Na⁺K⁺ ATPase expression (Figure 11A). We found that total protein expression did not change, indicating that A₂R induces intercellular adhesions involving recycled proteins. Notably, the movement of Na⁺K⁺ ATPase to the membrane is dependent on membrane localization of E-cadherin and coincides with the reorganization of cortical F-actin (55). Immunofluorescence

also showed an increase in membrane E-cadherin, β-catenin, and Na⁺K⁺ ATPase and lower cytoplasmic expression with CPA treatment (Figure 11, B–D).

Loss of CD73-generated adenosine promotes migration and invasion. We have shown that high-grade and advanced-stage endometrial carcinomas are associated with loss of CD73 and that CD73 is essential for protecting epithelial integrity (inducing the re-formation of cell-cell adhesions). We hypothesized that inhibition of CD73 in well-differentiated endometrial carcinoma cells would promote cellular migration and invasion in

Table 1. Migration and invasion with CD73 knockdown or with the CD73 inhibitor AoPCP

| Treatment | HEC-1-B, % Migration \pm SEM | HEC-1-B, % Invasion \pm SEM | HEC-1-A, % Migration \pm SEM |
|-----------------------|--------------------------------|---------------------------------|--------------------------------|
| Parental | 100.00 | 100.00 | 100.00 |
| Nontargeting siRNA | 89.00 \pm 6.10 | 123.90 \pm 8.58 | 122.10 \pm 23.34 |
| CD73 siRNA | 162.10 \pm 2.95 ^A | 182.10 \pm 6.67 ^A | 201.60 \pm 9.71 ^A |
| CD73 siRNA + NECA | 125.20 \pm 3.88 ^B | 117.70 \pm 11.93 ^B | 160.40 \pm 6.76 ^B |
| 5'-AMP | 100.00 | 100.00 | 100.00 |
| 5'-AMP + AoPCP | 173.90 \pm 3.59 ^A | 178.90 \pm 29.14 ^A | 232.10 \pm 9.71 ^A |
| 5'-AMP + AoPCP + NECA | 141.00 \pm 2.97 ^B | 108.50 \pm 7.14 ^B | 194.80 \pm 6.98 ^B |

^A*P* < 0.001 compared with nontargeting siRNA or 5'-AMP; and ^B*P* < 0.001 compared with CD73 siRNA or 5'-AMP plus AoPCP. *P* values were calculated by 1-way ANOVA with Tukey's post test. Data represent 2 independent experiments performed in triplicate.

vitro. We found that CD73 siRNA increased HEC-1-B cell migration and invasion by approximately 60% (Table 1) and HEC-1-A migration by approximately 80% (Table 1). HEC-1-A cells did not invade under 1% O₂, 5% CO₂ hypoxic conditions. Similarly, treatment of cells with the CD73 inhibitor AoPCP increased HEC-1-B cell migration and invasion by approximately 70% (Table 1), indicating that endometrial carcinoma cell migration and invasion is dependent on the loss of CD73-generated adenosine. We observed that AoPCP increased HEC-1-A cell migration by approximately 130% (Table 1). CD73 siRNA efficiency was approximately 90% (Supplemental Figure 16A), and AoPCP efficiencies for HEC-1-A and HEC-1-B cells are shown in Supplemental Figure 16B. We found that NECA reversed the effects of CD73 siRNA and AoPCP treatment (Table 1). Representative images are shown in Supplemental Figure 17.

Discussion

In the present study, we explored the effects of loss of CD73 in endometrial carcinoma. We showed that CD73-generated adenosine protects epithelial integrity in normal endometrium, that this physiological reflex is intact in early-stage endometrial carcinomas, and that loss of CD73 is associated with tumor progression. Additionally, we showed that CD73-generated adenosine protects epithelial integrity via adenosine receptor-mediated actin polymerization, which specifically involves A₁R (Figure 12).

CD73 is overexpressed in a number of human tumors, and previous studies have highlighted the detrimental role of extracellular adenosine in tumor progression. There are exceptions, including the findings that CD73 is downregulated in prostate (56) and laryngeal (57) carcinomas and with higher tumor grade in colon carcinomas (58), that CD73 overexpression is associated with well-differentiated tumors and better prognosis in ovarian carcinomas, and that CD73 expression is associated with both good and poor prognosis in breast cancer (59, 60). Endometrial carcinomas were recently reported to highly express CD73, but no difference in expression was seen between endometrial carcinomas and the adjacent benign endometrium (61). The tumors from this study were mainly FIGO stage I (*n* = 24 of 29). Our data showed that early-stage, specifically FIGO IA, tumors have CD73 expression comparable to that of normal, proliferative endometrium. To our knowledge, this is the first study to show a mechanistic basis for why CD73 loss in human cancer promotes

tumor progression. By providing evidence for the crucial role of CD73 loss in promoting tumor progression, we hope to pave the way for different perspectives regarding CD73 in cancer.

It has been suggested that epigenetic silencing of *CD73* in early-stage disease may abrogate differentiation and promote migration in a subset of melanomas (62). However, it is not clear whether CD73-generated adenosine protects cell-cell adhesions and epithelial integrity in other cancer types, as there are numerous examples of tissue- and cell-specific differences in the expression and function of CD73. In normal breast, CD73 is mostly absent from ductal and acinar epithelial cells, whereas myoepithelial cells express CD73 more frequently (63). High *CD73* expression levels are generally found in triple-negative breast cancer (TNBC) cell lines (i.e., MDA-MB-231 and MDA-MB-468; ref. 64) and in TNBC tumors compared with levels detected in other breast cancer cell lines (i.e., MCF-7 and T47D) and tumor subtypes, such as luminal and HER2⁺ tumors (3, 15). RNAi knockdown (9, 12) and CD73 Ab treatment (3) in TNBC breast cancer models decreased tumor growth and metastasis. TNBC and MDA-MB-231 cells both share gene expression signatures similar to those of basal/myoepithelial cells of the breast (65, 66). High expression levels of CD73 have also been related to certain stem cell populations in the mammary gland (67), so it is possible that high CD73 levels in TNBC is a major factor in promoting the aggressive, "stem-like" nature of these tumors. Thus, epithelial CD73 in different tissues may have distinct roles compared with those of endometrial epithelial cells. Accordingly, primary myoepithelial cells from normal human breast tissue exhibit a highly invasive capacity when grown at low density (66). There are regional differences in CD73 expression in epithelial cells of the gastrointestinal tract (41). Within the same tissue region, CD73 expression can also differ. In the ileum, villus absorptive cells do not express CD73, while crypt cells are positive (41). CD73 function can also differ in the same cell type from tissue to tissue. For example, CD73 in vascular endothelium regulates leukocyte trafficking, but does not affect leukocyte movement across lymphatic endothelium (42). In the immune system, naive T lymphocytes express CD73, but CD73 is absent on effector T cells (68) and is enriched intracellularly in Tregs (69). Functionally, these T cells respond to adenosine via A_{2A}R, but differ in their responses (effector cells are inactivated, while Treg activity increases) (70, 71). Similar heterogeneity is

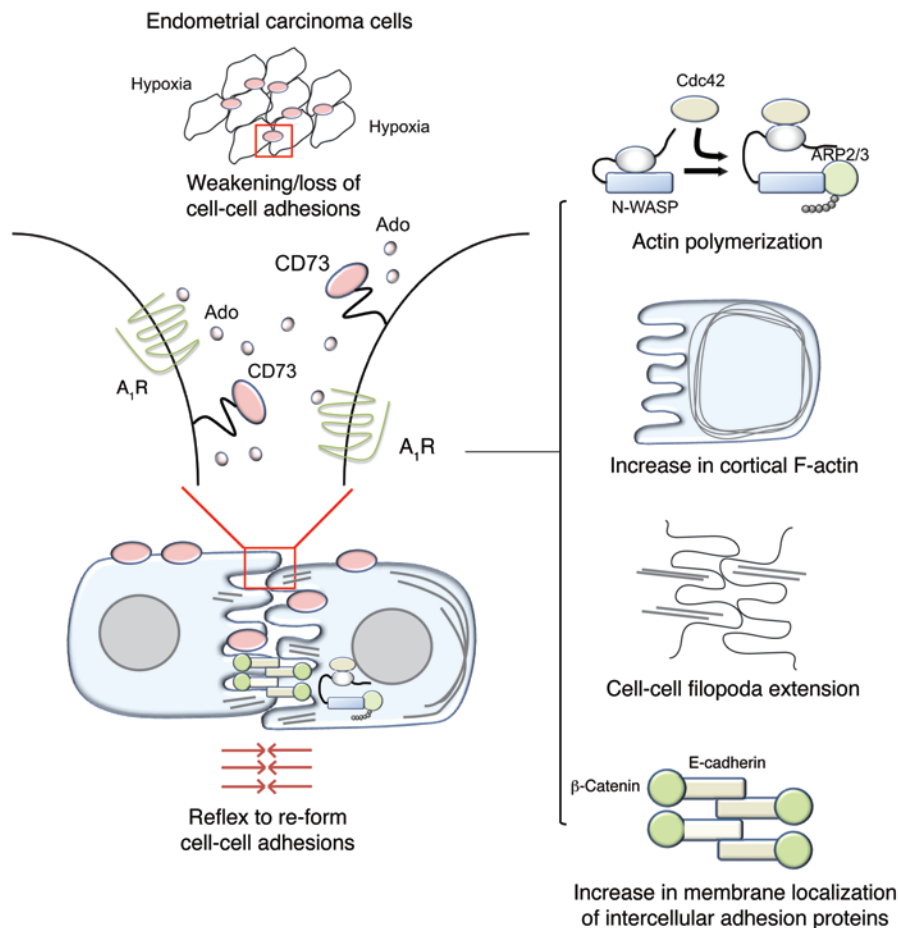


Figure 12. CD73-generated adenosine in endometrial carcinoma. Early-stage, well-differentiated endometrial carcinomas express high levels of CD73. Hypoxia weakens cell-cell adhesions and increases adenine nucleotides at the cell surface, supporting the generation of extracellular adenosine (Ado) by CD73. Extracellular adenosine activates A₁R, inducing actin polymerization, increasing circumferential cortical actin, and extending cell-cell filopodia. A₁R induces actin polymerization involving CDC42 and its conformational change of the ARP2/3 actin polymerization complex member N-WASP. Intercellular adhesion proteins E-cadherin and β-catenin increase at the membrane. Collectively, CD73-generated adenosine induces a physiological reflex to protect epithelial integrity. Downregulation of CD73 negates this reflex, promoting tumor cell migration and invasion.

seen in the expression of adenosine receptors, with different patterns observed for breast (refs. 3, 72 and Supplemental Figure 12) and colon (73, 74) epithelial cells, innate and adaptive immune cells (75), and endothelial cells (23, 76, 77).

Though CD73 loss promotes tumor progression in endometrial carcinoma, our finding that CD73-generated adenosine induces a physiological reflex to protect epithelial integrity is not far removed from the original thought by Ohta and Sitkovsky that extracellular adenosine protects cancerous tissue via its immunosuppressive actions (16). Extracellular adenosine/A_{2A}R signaling is a critical axis that limits inflammatory responses, protecting normal tissues from damage (18). Similarly, extracellular adenosine/A_{2A}R signaling on immune cells constitutes the basis of immune escape in tumors, protecting cancers by inhibiting the influx of antitumor T cells (16). Many nonimmune-related actions of CD73 promote tumor progression. However, the potent immunosuppressive action of extracellular adenosine is the major factor in CD73-mediated tumor progression (3–8). This is highlighted by studies showing that CD73-deficient mice resist tumor growth and experimental metastasis in many cancer models, largely because of CD8⁺ T cells (5–7). Immune escape is attributed to CD73 expression in both tumor and nontumor cells (3–8). We observed no change in CD73 expression levels in the stromal cells of endometrial tumors by immunofluorescence. It is certainly possible that nontumor-cell CD73 mediates tumor progression. Tumor resis-

tance in CD73-deficient mice does not correlate with CD73 expression on tumor cells (5). The generation of extracellular adenosine for epithelial integrity could simultaneously induce immunosuppression as well. In tumors with seemingly opposing CD73 actions, deciphering the mechanisms underlying these events in the presence of tumor–host cell interactions will be critical to understanding which adenosine-regulated responses predominate. Interestingly, high densities of CD8⁺ cells were recently associated with poor prognosis in prostate cancers in which CD73 was expressed at high levels in adjacent normal prostate epithelium (78). The authors suggest that this CD73 expression may provide immune escape by converting surveying CD8⁺ T cells into immunosuppressive cells (78).

We found in the immunoresponsive TCGA subset of endometrial carcinomas (characterized by higher expression levels of immune response-related genes) that CD73 expression levels were significantly lower compared with those in the hormonal subset (characterized by higher expression levels of hormone receptors and genes induced by estrogen; Supplemental Figure 1C). Genes that characterize the immunoresponsive subset (*CD74*, *CD14*, *TNFRSF1B*, and *CEBPD*) have been shown to both activate and suppress immune responses (79–84). No differences in inflammatory cell infiltrates were seen in the different endometrial carcinoma subtypes (Supplemental Figure 4.7 in ref. 33), although different lymphocyte populations were not assessed. Future studies are necessary to understand the signif-

importance of lower *CD73* expression levels in this cancer subtype. It is reasonable to hypothesize that *CD73*-mediated cell-cell adhesions may be indirectly immunosuppressive. The role of *CD73*-mediated cell-cell adhesion in tumors is comparable to that of *CD73* in maintaining barrier function in the gut (25). In the gut, breakdown of the intestinal epithelial cell barrier contributes to the development of colitis and inflammatory bowel disease (85). Thus, in both colitis and endometrial cancer, a major determinant of disease severity is loss of epithelial cell *CD73* (74, 86, 87). Damage to the epithelial barrier results in the production of inflammatory mediators by immune cells and epithelial cells (88). Inducing epithelial integrity in the early stages of disease may be a way to protect the developing/growing tumor from its own induction of proinflammatory and antitumor immune actions triggered by damage to the epithelial barrier. *CD73*-induced cell-cell adhesions may therefore be immunosuppressive simply by acting as a physiological barrier. This possibility or the importance of *CD73* expression on nontumor cells in endometrial carcinoma cannot be determined on the basis of our study. The relative contribution of tumor versus stromal and immune cell *CD73* and the interaction of cell types in the tumor microenvironment are likely different for different tumor types.

Increased extracellular adenosine in tumors (16, 26) is linked to hypoxia (89). *CD73* and $A_{2B}R$ upregulation by HIF-1 α promotes barrier function (25, 47), yet *CD73* expression was not induced by hypoxia in HEC-1-A or HEC-1-B cells, which suggests an escape mechanism of endometrial carcinoma cells to de-link hypoxia from *CD73* upregulation. Notably, the full-length promoter of *CD73* contains an area that represses *CD73* expression in hypoxia (25). We found that $A_{2B}R$ expression was not uncoupled from hypoxia upregulation. We thus hypothesize that $A_{2B}R$ may counterbalance A_1R -mediated actin polymerization. Endometrial carcinomas appear to avoid extracellular adenosine overall, as alkaline phosphatase, another source of extracellular adenosine, is downregulated in poorly differentiated and advanced-stage endometrial carcinomas (90, 91). *ENT1*, a bidirectional transporter mediating adenosine efflux or intracellular uptake according to the direction of the concentration gradient (92), was also downregulated in advanced-stage endometrial tumors ($P < 0.02$, Supplemental Table 1), and its expression was positively correlated with that of *CD73* ($P < 0.0001$, Pearson's $r = 0.7010$). With *CD73* loss, the concomitant loss of *ENT1* would be expected to prevent the movement of higher concentrations of intracellular adenosine to the extracellular space. Decreased adenosine uptake due to *ENT1* downregulation via HIF-1 α induces vascular barrier protection (93). Similarly, in tumor types that maintain expression of *CD73*, *ENT1* downregulation may help protect epithelial integrity by allowing increased extracellular adenosine (93).

$A_{2B}R$ has been the primary adenosine receptor shown to protect endothelial and intestinal epithelial integrity and promote barrier function (22, 23, 94–96). $A_{2B}R$ -deficient mice failed to show a significant difference in epithelial barrier function in normal endometrium (Supplemental Figure 18). A_1R is the primary adenosine receptor mediating barrier function in vasa vasorum endothelial cells (VVECs) (77). Similar to endometrial carcinoma cells, VVECs express A_1R at higher levels than do other adenosine receptors (77). In VVECs, A_1R -mediated barrier function

involves actin cytoskeletal rearrangement (77). We showed that A_1R induces cortical actin polymerization and extension of cell-cell filopodia for cell-cell adhesions. Actin polymerization is a relatively fast biological action, and the regulation of actin polymerization by extracellular adenosine is consistent with the quick actions needed to re-form cell-cell adhesions and re-seal the barrier. These findings are supported by results from other studies (77, 97, 98). It is likely that *CD73*/adenosine receptor-mediated actin polymerization is also important in re-forming intercellular adhesions in endothelial cells, as filopodia-like protrusions connected by VE-cadherin-rich junctions have been reported in human umbilical vein endothelial cells (99).

Actin polymerization in cells is balanced by actions (induction of kinases, phosphatases, and actin depolymerization factors) that are induced shortly afterward to keep the actin polymerization response self-limiting (100). We found that treatment with NECA did not significantly affect F-actin, but NECA plus MRS1754 increased F-actin, suggesting that $A_{2B}R$ may counterbalance the actions of A_1R . This regulation may involve $A_{2B}R$ -mediated activity of vasodilator-stimulated phosphoprotein (VASP). For example, $A_{2B}R$ increases cAMP (101), whereas cAMP interferes with the formation of membrane protrusions (102). Barrier function in colon epithelial (95) and endothelial (94) cells has been associated with NECA-induced, cAMP-dependent kinase, protein kinase A-mediated (PKA-mediated) VASP phosphorylation (Ser 157), and localization of VASP to tight junctions (94, 95). VASP, besides regulating tight junctions, is involved in actin polymerization, specifically, the nucleation, bundling, and capping of actin filaments (103). PKA phosphorylation of VASP (Ser 153 in mice, corresponding to Ser 157 in humans) inhibits both actin nucleation and VASP interaction with actin filaments (104). We showed that A_1R induces actin polymerization involving the CDC42 and ARP2/3 complex member N-WASP. VASP enhances actin nucleation mediated via the ARP2/3 complex (105). This sort of coordination would be similar to that observed for different adenosine receptors in the initiation and then suppression of inflammatory responses in tissues to keep the immune response self-limited (106). Though specific $A_{2B}R$ agonists are not widely available at this time, the possibility that A_1R -mediated actin polymerization is counterbalanced by $A_{2B}R$ merits further investigation, especially considering that a number of endothelial and epithelial cells express both A_1R and $A_{2B}R$ (77, 107, 108).

In summary, loss of *CD73* in endometrial carcinoma is crucial to tumor progression, as it negates the physiological reflex of extracellular adenosine to protect epithelial integrity. Our finding that loss of *CD73* promotes tumor progression is counter to the current understanding of *CD73* in cancer, but consistent with reports on other types of cancer. This study highlights the complex biology of *CD73* and extracellular adenosine in human tumors. Understanding the multiple facets of *CD73* in cancer will be important to the future clinical success of *CD73*-targeted therapeutics.

Methods

See the Supplemental Methods for details on $A_{2B}R^{-/-}$ mice; H&E, immunofluorescence, phalloidin, and annexin V-FITC propidium iodide staining; ecto-AMPase activity; transmission electron microscopy; immunoblotting; siRNA transfection; and cell migration and invasion.

Human tissues. EECs, proliferative-phase endometrium, ovarian HGSCs, and N-Ovaries were obtained from the Department of Pathology of the MD Anderson Cancer Center as residual tissues from hysterectomies. For surgical staging details, see Supplemental Table 2.

Mice. *Cd73*^{-/-} mice (24) were provided by Linda Thompson (Oklahoma Medical Research Foundation, Oklahoma City, Oklahoma, USA) and were maintained on a C57BL/6 background (Harlan Laboratories). Mice were maintained in a 12-hour light/12-hour dark cycle, and female mice estrous cycles were synchronized beginning at 8 weeks of age.

Cell lines. HEC-1-A and HEC-1-B cells (American Type Culture Collection [ATCC]) were maintained according to ATCC recommendations and authenticated by short tandem repeat DNA profiling. Details on all other cell lines used are provided in the Supplemental Methods.

Reagents and Abs. All reagents were purchased from Sigma-Aldrich, unless otherwise indicated. DCF and MRS1754 were from Tocris Biosciences. Human recombinant CD73 was from R&D Systems. 5'-Nucleotidase from *Crotalus atrox* venom was purchased from Sigma-Aldrich (catalog N8661). The complete list of Abs used is provided in Supplemental Table 3.

Plasmids. pRK5-Myc-CDC42 was a gift of Gary Bokoch (Addgene plasmid 12972). WASL Myc-DDK-tagged Wiskott-Aldrich syndrome-like (WASL, alternatively called N-WASP) was purchased from OriGene (catalog RC207967). Plasmids were propagated in *E. coli* DH5 α and purified on QIAGEN-tip 100 columns (QIAGEN).

RNA extraction and real-time quantitative PCR. RNA was isolated from frozen tissues using TRIzol Reagent (Invitrogen), followed by purification with RNeasy columns (QIAGEN). RNA was isolated from cell lines using Quick-RNA MiniPrep columns (Zymo Research). Details on real-time quantitative PCR (qPCR), assay development, and data analysis are provided in the Supplemental Methods. For the list of primers used and probe sequences, see Supplemental Table 4.

Ruthenium red uterine perfusions. Ten- to fourteen-week-old mice in proestrus were individually placed in a modular incubator chamber (Billups-Rothenberg) and exposed to room air or hypoxia (7% O₂) for 4 hours. The proestrus period was selected because of its higher CD73 expression levels in luminal and glandular uterine epithelial cells (109). Additionally, membrane localization of tight-junction proteins increases in rodent uterine epithelial cells during proestrus (110). Following exposure to room air or hypoxia, mice were anesthetized with 0.2 ml/10 g tribromoethanol, and a peritoneal incision was made. Uterine horns were perfusion fixed with 0.2 ml 0.2% ruthenium red and 2% glutaraldehyde in 0.1 M sodium cacodylate buffer and then filled with 0.1 ml 0.2% ruthenium red and 2% glutaraldehyde in 0.1 M sodium cacodylate buffer following closure of the endocervical canal with a surgical thread knot. Anesthetized mice were returned to the chambers for 10 minutes. After removal of the surgical thread, the uterine horns were reperused, in order, with 0.7 ml 0.2% ruthenium red and 2% glutaraldehyde in 0.1 M sodium cacodylate buffer and 0.2 ml 0.2% ruthenium red in 2% osmium tetroxide in 0.1 M sodium cacodylate buffer. In additional studies, *Cd73*^{-/-} mice were injected i.p. with NECA 0.1 mg/kg or DMSO prior to being exposed to hypoxia for 4 hours. Dosing and administration of NECA to *Cd73*^{-/-} mice was similar to that described previously (24).

Isolation of total actin. Total actin was isolated using a G-actin/F-actin In Vivo Assay Biochem Kit (Cytoskeleton). Ultracentrifugation was performed using a Beckman Coulter Optima Max-XP Ultracentrifuge with a Beckman Coulter TLS-55 rotor.

Co-IP. HEC-1-A cells were transfected with pRK5-Myc-CDC42 or pCMV6-Myc-NWASP (2 μ g) in serum-free Opti-MEM (Invitrogen) using Lipofectamine 2000 (Invitrogen). HEC-1-A cells were treated with 10 μ M CPA or DMSO in hypoxia (1% O₂, 5%) for 36 hours, 24 hours after transfection. Co-IP was performed using a Pierce c-Myc-Tag Magnetic IP/Co-IP Kit (Thermo Scientific). Protein (1 mg) was incubated overnight at 4°C with 25 μ l anti-Myc magnetic beads. The resulting immune-bound complexes were eluted in 2X reducing sample buffer and assessed by SDS-PAGE using a 4%–12% gradient polyacrylamide gel (BioRad) and immunoblotting methods.

Cellular fractionation. Cellular fractions were isolated using a Pierce Subcellular Protein Fractionation Kit (Thermo Scientific). Fractions were concentrated using Amicon Ultra Centrifugal Filters (EMD Millipore).

Statistics. *P* values were calculated using an unpaired *t* test, 1-way ANOVA with Tukey's post test, 2-way ANOVA with Bonferroni's post test, or as otherwise indicated (GraphPad Prism 6; GraphPad Software). Human tissue data were analyzed using a Mann-Whitney *U* test or Kruskal-Wallis 1-way ANOVA with Dunn's post test. A *P* value of less than 0.05 was considered significant. Survival data were collected by review of electronic medical records, and overall survival rates were stratified in a Kaplan-Meier plot according to *CD73* mRNA levels.

Study approval. Use of human tissues was approved by the IRB of the University of Texas MD Anderson Cancer Center (LAB01-718). Animal studies were approved by the IACUC of the University of Texas Medical School at Houston.

Author contributions

JLB and RRB developed the study concept and design. JLB performed experiments and analyzed the data, and JLB, MRB, and RRB interpreted the data. GLS performed the real-time qPCR studies. JGM bred and genotyped the mice. KD provided expertise on transmission electron microscopy. JLB and RRB wrote the manuscript.

Acknowledgments

We thank Linda Thompson for providing the *Cd73*^{-/-} mice; Steven Curly, Andrew Gladden, and Samuel Mok for providing equipment; Carolyn Hall for helpful discussions; and Jiping Feng for technical assistance. Yuexin Liu provided the *CD73* expression data from TCGA endometrial cancer project. This work was supported by NIH grant P50CA098258 (Uterine Cancer SPORE, to R.R. Broaddus); NIH grant TL1RR024147 from the National Center for Research Resources (to J.L. Bowser); the Interdisciplinary Translational Education and Research Training Program (to J.L. Bowser) in the Department of Translational Molecular Pathology; and the University of Texas MD Anderson Cancer Center NIH Cancer Center Support Grant P30CA016672.

Address correspondence to: Russell R. Broaddus, Department of Pathology, Box 85, University of Texas MD Anderson Cancer Center, 1515 Holcombe Blvd., Houston, Texas 77030, USA. Phone: 713.745.2794; E-mail: rbroadus@mdanderson.org.

1. Zimmermann H. 5'-Nucleotidase: molecular structure and functional aspects. *Biochem J*. 1992;285(pt 2):345-365.
2. Antonioli L, Pacher P, Vizi ES, Hasko G. CD39 and CD73 in immunity and inflammation. *Trends Mol Med*. 2013;19(6):355-367.
3. Stagg J, et al. Anti-CD73 antibody therapy inhibits breast tumor growth and metastasis. *Proc Natl Acad Sci U S A*. 2010;107(4):1547-1552.
4. Jin D, et al. CD73 on tumor cells impairs anti-tumor T-cell responses: a novel mechanism of tumor-induced immune suppression. *Cancer Res*. 2010;70(6):2245-2255.
5. Stagg J, et al. CD73-deficient mice have increased antitumor immunity and are resistant to experimental metastasis. *Cancer Res*. 2011;71(8):2892-2900.
6. Wang L, et al. CD73 has distinct roles in non-hematopoietic and hematopoietic cells to promote tumor growth in mice. *J Clin Invest*. 2011;121(6):2371-2382.
7. Yegutkin GG, et al. Altered purinergic signaling in CD73-deficient mice inhibits tumor progression. *Eur J Immunol*. 2011;41(5):1231-1241.
8. Stagg J, et al. CD73-deficient mice are resistant to carcinogenesis. *Cancer Res*. 2012;72(9):2190-2196.
9. Zhi X, et al. RNA interference of ecto-5'-nucleotidase (CD73) inhibits human breast cancer cell growth and invasion. *Clin Exp Metastasis*. 2007;24(6):439-448.
10. Zhou P, et al. Overexpression of Ecto-5'-nucleotidase (CD73) promotes T-47D human breast cancer cells invasion and adhesion to extracellular matrix. *Cancer Biol Ther*. 2007;6(3):426-431.
11. Wang L, et al. Ecto-5'-nucleotidase promotes invasion, migration and adhesion of human breast cancer cells. *J Cancer Res Clin Oncol*. 2008;134(3):365-372.
12. Zhi X, et al. RNAi-mediated CD73 suppression induces apoptosis and cell-cycle arrest in human breast cancer cells. *Cancer Sci*. 2010;101(12):2561-2569.
13. Ujhazy P, et al. Evidence for the involvement of ecto-5'-nucleotidase (CD73) in drug resistance. *Int J Cancer*. 1996;68(4):493-500.
14. Quezada C, et al. 5'-ectonucleotidase mediates multiple-drug resistance in glioblastoma multiforme cells. *J Cell Physiol*. 2013;228(3):602-608.
15. Loi S, et al. CD73 promotes anthracycline resistance and poor prognosis in triple negative breast cancer. *Proc Natl Acad Sci U S A*. 2013;110(27):11091-11096.
16. Ohta A, et al. A2A adenosine receptor protects tumors from antitumor T cells. *Proc Natl Acad Sci U S A*. 2006;103(35):13132-13137.
17. Colgan SP, Eltzschig HK, Eckle T, Thompson LF. Physiological roles for ecto-5'-nucleotidase (CD73). *Purinergic Signal*. 2006;2(2):351-360.
18. Ohta A, Sitkovsky M. Role of G-protein-coupled adenosine receptors in downregulation of inflammation and protection from tissue damage. *Nature*. 2001;414(6866):916-920.
19. Linden J. Adenosine in tissue protection and tissue regeneration. *Mol Pharmacol*. 2005;67(5):1385-1387.
20. Madara JL, et al. 5'-adenosine monophosphate is the neutrophil-derived paracrine factor that elicits chloride secretion from T84 intestinal epithelial cell monolayers. *J Clin Invest*. 1993;91(5):2320-2325.
21. Eckle T, et al. Cardioprotection by ecto-5'-nucleotidase (CD73) and A2B adenosine receptors. *Circulation*. 2007;115(12):1581-1590.
22. Lennon PF, Taylor CT, Stahl GL, Colgan SP. Neutrophil-derived 5'-adenosine monophosphate promotes endothelial barrier function via CD73-mediated conversion to adenosine and endothelial A2B receptor activation. *J Exp Med*. 1998;188(8):1433-1443.
23. Eltzschig HK, et al. Coordinated adenine nucleotide phosphohydrolysis and nucleoside signaling in posthypoxic endothelium: role of ectonucleotidases and adenosine A2B receptors. *J Exp Med*. 2003;198(5):783-796.
24. Thompson LF, et al. Crucial role for ecto-5'-nucleotidase (CD73) in vascular leakage during hypoxia. *J Exp Med*. 2004;200(11):1395-1405.
25. Synnestvedt K, et al. Ecto-5'-nucleotidase (CD73) regulation by hypoxia-inducible factor-1 mediates permeability changes in intestinal epithelia. *J Clin Invest*. 2002;110(7):993-1002.
26. Blay J, White TD, Hoskin DW. The extracellular fluid of solid carcinomas contains immunosuppressive concentrations of adenosine. *Cancer Res*. 1997;57(13):2602-2605.
27. Wang L, et al. Ecto-5'-nucleotidase (CD73) promotes tumor angiogenesis. *Clin Exp Metastasis*. 2013;30(5):671-680.
28. Allard B, Turcotte M, Spring K, Pommey S, Royal I, Stagg J. Anti-CD73 therapy impairs tumor angiogenesis. *Int J Cancer*. 2014;134(6):1466-1473.
29. Koszalka P, et al. Inhibition of CD73 stimulates the migration and invasion of B16F10 melanoma cells in vitro, but results in impaired angiogenesis and reduced melanoma growth in vivo. *Oncol Rep*. 2014;31(2):819-827.
30. Allard B, Turcotte M, Stagg J. CD73-generated adenosine: orchestrating the tumor-stroma interplay to promote cancer growth. *J Biomed Biotechnol*. 2012;2012:485156.
31. Silverberg SG. Problems in the differential diagnosis of endometrial hyperplasia and carcinoma. *Mod Pathol*. 2000;13(3):309-327.
32. Hendrickson M, Ross J, Eifel P, Martinez A, Kempson R. Uterine papillary serous carcinoma: a highly malignant form of endometrial adenocarcinoma. *Am J Surg Pathol*. 1982;6(2):93-108.
33. Kandath C, et al. Integrated genomic characterization of endometrial carcinoma. *Nature*. 2013;497(7447):67-73.
34. Kuramoto H, Tamura S, Notake Y. Establishment of a cell line of human endometrial adenocarcinoma in vitro. *Am J Obstet Gynecol*. 1972;114(8):1012-1019.
35. Mayor S, Riezman H. Sorting GPI-anchored proteins. *Nat Rev Mol Cell Biol*. 2004;5(2):110-120.
36. Partridge MA, Marcantonio EE. Initiation of attachment and generation of mature focal adhesions by integrin-containing filopodia in cell spreading. *Mol Biol Cell*. 2006;17(10):4237-4248.
37. Galbraith CG, Yamada KM, Galbraith JA. Polymerizing actin fibers position integrins primed to probe for adhesion sites. *Science*. 2007;315(5814):992-995.
38. Yonemura S, Itoh M, Nagafuchi A, Tsukita S. Cell-to-cell adherens junction formation and actin filament organization: similarities and differences between non-polarized fibroblasts and polarized epithelial cells. *J Cell Sci*. 1995;108(pt 1):127-142.
39. Vasioukhin V, Bauer C, Yin M, Fuchs E. Directed actin polymerization is the driving force for epithelial cell-cell adhesion. *Cell*. 2000;100(2):209-219.
40. Costa M, Raich W, Agbunag C, Leung B, Hardin J, Priess JR. A putative catenin-cadherin system mediates morphogenesis of the *Caenorhabditis elegans* embryo. *J Cell Biol*. 1998;141(1):297-308.
41. Raich WB, Agbunag C, Hardin J. Rapid epithelial-sheet sealing in the *Caenorhabditis elegans* embryo requires cadherin-dependent filopodial priming. *Curr Biol*. 1999;9(20):1139-1146.
42. Tanaka-Matakatsumi M, Uemura T, Oda H, Takeichi M, Hayashi S. Cadherin-mediated cell adhesion and cell motility in *Drosophila* trachea regulated by the transcription factor Escargot. *Development*. 1996;122(12):3697-3705.
43. Martin-Blanco E, Pastor-Pareja JC, Garcia-Bellido A. JNK and decapentaplegic signaling control adhesiveness and cytoskeleton dynamics during thorax closure in *Drosophila*. *Proc Natl Acad Sci U S A*. 2000;97(14):7888-7893.
44. Jacinto A, Wood W, Balayo T, Turmaine M, Martinez-Arias A, Martin P. Dynamic actin-based epithelial adhesion and cell matching during *Drosophila* dorsal closure. *Curr Biol*. 2000;10(22):1420-1426.
45. Vasioukhin V, Fuchs E. Actin dynamics and cell-cell adhesion in epithelia. *Curr Opin Cell Biol*. 2001;13(1):76-84.
46. Pansare V, et al. Increased expression of hypoxia-inducible factor 1alpha in type I and type II endometrial carcinomas. *Mod Pathol*. 2007;20(1):35-43.
47. Kong T, Westerman KA, Faigle M, Eltzschig HK, Colgan SP. HIF-dependent induction of adenosine A2B receptor in hypoxia. *FASEB J*. 2006;20(13):2242-2250.
48. Linden J. Molecular approach to adenosine receptors: receptor-mediated mechanisms of tissue protection. *Annu Rev Pharmacol Toxicol*. 2001;41:775-787.
49. Nachmias VT, Philp N, Momoyama Y, Choi JK. G-actin pool and actin messenger RNA during development of the apical processes of the retinal pigment epithelial cells of the chick. *Dev Biol*. 1992;149(2):239-246.
50. Lewis JE, et al. Cross-talk between adherens junctions and desmosomes depends on plakoglobin. *J Cell Biol*. 1997;136(4):919-934.
51. Takenawa T, Suetsugu S. The WASP-WAVE protein network: connecting the membrane to the cytoskeleton. *Nat Rev Mol Cell Biol*. 2007;8(1):37-48.
52. Nobes CD, Hall A. Rho, rac, and cdc42 GTPases regulate the assembly of multimolecular focal complexes associated with actin stress fibers, lamellipodia, and filopodia. *Cell*. 1995;81(1):53-62.
53. Miki H, Sasaki T, Takai Y, Takenawa T. Induction

- of filopodium formation by a WASP-related actin-depolymerizing protein N-WASP. *Nature*. 1998;391(6662):93–96.
54. Rohatgi R, et al. The interaction between N-WASP and the Arp2/3 complex links Cdc42-dependent signals to actin assembly. *Cell*. 1999;97(2):221–231.
 55. McNeill H, Ozawa M, Kemler R, Nelson WJ. Novel function of the cell adhesion molecule uvomorulin as an inducer of cell surface polarity. *Cell*. 1990;62(2):309–316.
 56. Rackley RR, et al. 5'-nucleotidase activity in prostatic carcinoma and benign prostatic hyperplasia. *Cancer Res*. 1989;49(13):3702–3707.
 57. Durak I, Isik AC, Canbolat O, Akyol O, Kavutcu M. Adenosine deaminase, 5' nucleotidase, xanthine oxidase, superoxide dismutase, and catalase activities in cancerous and noncancerous human laryngeal tissues. *Free Radic Biol Med*. 1993;15(6):681–684.
 58. Eroglu A, Canbolat O, Demirci S, Kocaoglu H, Eryavuz Y, Akgül H. Activities of adenosine deaminase and 5'-nucleotidase in cancerous and noncancerous human colorectal tissues. *Med Oncol*. 2000;17(4):319–324.
 59. Leth-Larsen R, et al. Metastasis-related plasma membrane proteins of human breast cancer cells identified by comparative quantitative mass spectrometry. *Mol Cell Proteomics*. 2009;8(6):1436–1449.
 60. Supernat A, et al. CD73 expression as a potential marker of good prognosis in breast carcinoma. *Appl Immunohistochem Mol Morphol*. 2012;20(2):103–107.
 61. Aliagas E, Vidal A, Texido L, Ponce J, Condom E, Martin-Satue M. High expression of ecto-nucleotidases CD39 and CD73 in human endometrial tumors. *Mediators Inflamm*. 2014;2014:509027.
 62. Wang H, et al. NT5E (CD73) is epigenetically regulated in malignant melanoma and associated with metastatic site specificity. *Br J Cancer*. 2012;106(8):1446–1452.
 63. Kruger KH, Thompson LF, Kaufmann M, Moller P. Expression of ecto-5'-nucleotidase (CD73) in normal mammary gland and in breast carcinoma. *Br J Cancer*. 1991;63(1):114–118.
 64. Zhi X, Wang Y, Yu J, Zhang L, Yin L, Zhou P. Potential prognostic biomarker CD73 regulates epidermal growth factor receptor expression in human breast cancer. *IUBMB Life*. 2012;64(11):911–920.
 65. Sorlie T, et al. Gene expression patterns of breast carcinomas distinguish tumor subclasses with clinical implications. *Proc Natl Acad Sci U S A*. 2001;98(19):10869–10874.
 66. Gordon LA, Mulligan KT, Maxwell-Jones H, Adams M, Walker RA, Jones JL. Breast cell invasive potential relates to the myoepithelial phenotype. *Int J Cancer*. 2003;106(1):8–16.
 67. Roy S, et al. Rare somatic cells from human breast tissue exhibit extensive lineage plasticity. *Proc Natl Acad Sci U S A*. 2013;110(12):4598–4603.
 68. Bono MR, Fernandez D, Flores-Santibanez F, Roseblatt M, Sauma D. CD73 and CD39 ectonucleotidases in T cell differentiation: beyond immunosuppression. *FEBS Lett*. 2015;589(22):3454–3560.
 69. Mandapathil M, et al. Generation and accumulation of immunosuppressive adenosine by human CD4⁺CD25^{high}FOXP3⁺ regulatory T cells. *J Biol Chem*. 2010;285(10):7176–7186.
 70. Ohta A, Kini R, Ohta A, Subramanian M, Madasu M, Sitkovsky M. The development and immunosuppressive functions of CD4(+) CD25(+) FoxP3(+) regulatory T cells are under influence of the adenosine-A2A adenosine receptor pathway. *Front Immunol*. 2012;3:190.
 71. Ohta A, Sitkovsky M. Extracellular adenosine-mediated modulation of regulatory T cells. *Front Immunol*. 2014;5:304.
 72. Panjehpour M, Castro M, Klotz KN. Human breast cancer cell line MDA-MB-231 expresses endogenous A2B adenosine receptors mediating a Ca²⁺ signal. *Br J Pharmacol*. 2005;145(2):211–218.
 73. Strohmeier GR, Reppert SM, Lencer WI, Madara JL. The A2b adenosine receptor mediates cAMP responses to adenosine receptor agonists in human intestinal epithelia. *J Biol Chem*. 1995;270(5):2387–2394.
 74. Louis NA, Robinson AM, MacManus CF, Karhausen J, Scully M, Colgan SP. Control of IFN- α A by CD73: implications for mucosal inflammation. *J Immunol*. 2008;180(6):4246–4255.
 75. Burnstock G, Boeynaems JM. Purinergic signalling and immune cells. *Purinergic Signal*. 2014;10(4):529–564.
 76. Feoktistov I, et al. Differential expression of adenosine receptors in human endothelial cells: role of A2B receptors in angiogenic factor regulation. *Circ Res*. 2002;90(5):531–538.
 77. Umapathy SN, et al. Adenosine A1 receptors promote vasa vasorum endothelial cell barrier integrity via Gi and Akt-dependent actin cytoskeleton remodeling. *PLoS One*. 2013;8(4):e59733.
 78. Leclerc BG, et al. CD73 expression is an independent prognostic factor in prostate cancer [published online ahead of print August 7, 2015]. *Clin Cancer Res*. doi:10.1158/1078-0432.CCR-15-1181.
 79. Borghese F, Clanchy FI. CD74: an emerging opportunity as a therapeutic target in cancer and autoimmune disease. *Expert Opin Ther Targets*. 2011;15(3):237–251.
 80. Linke B, et al. The tolerogenic function of annexins on apoptotic cells is mediated by the annexin core domain. *J Immunol*. 2015;194(11):5233–5242.
 81. Hsiao YW, et al. CCAAT/enhancer binding protein delta in macrophages contributes to immunosuppression and inhibits phagocytosis in nasopharyngeal carcinoma. *Sci Signal*. 2013;6(284):ra59.
 82. Stein R, et al. CD74: a new candidate target for the immunotherapy of B-cell neoplasms. *Clin Cancer Res*. 2007;13(18 pt 2):5556s–5563s.
 83. Cheah MT, et al. CD14-expressing cancer cells establish the inflammatory and proliferative tumor microenvironment in bladder cancer. *Proc Natl Acad Sci U S A*. 2015;112(15):4725–4730.
 84. Bremer E. Targeting of the tumor necrosis factor receptor superfamily for cancer immunotherapy. *ISRN Oncol*. 2013;2013:371854.
 85. Karrasch T, Jobin C. Wound healing responses at the gastrointestinal epithelium: a close look at novel regulatory factors and investigative approaches. *Zeitschrift fur Gastroenterologie*. 2009;47(12):1221–1229.
 86. Karhausen J, Furuta GT, Tomaszewski JE, Johnson RS, Colgan SP, Haase VH. Epithelial hypoxia-inducible factor-1 is protective in murine experimental colitis. *J Clin Invest*. 2004;114(8):1098–1106.
 87. Bynoe MS, Waickman AT, Mahamed DA, Mueller C, Mills JH, Czopik A. CD73 is critical for the resolution of murine colonic inflammation. *J Biomed Biotechnol*. 2012;2012:260983.
 88. Turner JR. Intestinal mucosal barrier function in health and disease. *Nat Rev Immunol*. 2009;9(11):799–809.
 89. Hatfield SM, et al. Immunological mechanisms of the antitumor effects of supplemental oxygenation. *Sci Transl Med*. 2015;7(277):277ra30.
 90. Atkinson WB, Gusberg SB. Histochemical studies on abnormal growth of human endometrium; alkaline phosphatase in hyperplasia and adenocarcinoma. *Cancer*. 1948;1(2):248–251.
 91. Nozawa S, et al. Heat-stable alkaline phosphatase in uterine cancer, with special reference to its histochemical heat-stability and the L-phenylalanine inhibition test. *Histochem J*. 1981;13(6):941–951.
 92. Löffler M, Morote-Garcia JC, Eltzschig SA, Coe IR, Eltzschig HK. Physiological roles of vascular nucleoside transporters. *Arterioscler Thromb Vasc Biol*. 2007;27(5):1004–1013.
 93. Eltzschig HK, et al. HIF-1-dependent repression of equilibrative nucleoside transporter (ENT) in hypoxia. *J Exp Med*. 2005;202(11):1493–1505.
 94. Comerford KM, Lawrence DW, Synnestvedt K, Levi BP, Colgan SP. Role of vasodilator-stimulated phosphoprotein in PKA-induced changes in endothelial junctional permeability. *FASEB J*. 2002;16(6):583–585.
 95. Lawrence DW, Comerford KM, Colgan SP. Role of VASP in reestablishment of epithelial tight junction assembly after Ca²⁺ switch. *Am J Physiol Cell Physiol*. 2002;282(6):C1235–C1245.
 96. Aherne CM, et al. Epithelial-specific A2B adenosine receptor signaling protects the colonic epithelial barrier during acute colitis. *Mucosal Immunol*. 2015;8(3):699.
 97. Panther E, et al. Expression and function of adenosine receptors in human dendritic cells. *FASEB J*. 2001;15(11):1963–1970.
 98. Kim M, Chen SW, Park SW, D'Agati VD, Yang J, Lee HT. Kidney-specific reconstitution of the A1 adenosine receptor in A1 adenosine receptor knockout mice reduces renal ischemia-reperfusion injury. *Kidney Int*. 2009;75(8):809–823.
 99. Hoelzle MK, Svitkina T. The cytoskeletal mechanisms of cell-cell junction formation in endothelial cells. *Mol Biol Cell*. 2012;23(2):310–323.
 100. Hotulainen P, et al. Defining mechanisms of actin polymerization and depolymerization during dendritic spine morphogenesis. *J Cell Biol*. 2009;185(2):323–339.
 101. Fredholm BB, IJzerman AP, Jacobson KA, Klotz KN, Linden J. International Union of Pharmacology. XXV. Nomenclature and classification of adenosine receptors. *Pharmacol Rev*. 2001;53(4):527–552.
 102. Chen L, Zhang JJ, Huang XY. cAMP inhibits cell migration by interfering with Rac-induced

- lamellipodium formation. *J Biol Chem.* 2008;283(20):13799–13805.
103. Krause M, Dent EW, Bear JE, Loureiro JJ, Gertler FB. Ena/VASP proteins: regulators of the actin cytoskeleton and cell migration. *Annu Rev Cell Dev Biol.* 2003;19:541–564.
104. Harbeck B, Huttelmaier S, Schluter K, Jockusch BM, Illenberger S. Phosphorylation of the vasodilator-stimulated phosphoprotein regulates its interaction with actin. *J Biol Chem.* 2000;275(40):30817–30825.
105. Skoble J, Auerbuch V, Goley ED, Welch MD, Portnoy DA. Pivotal role of VASP in Arp2/3 complex-mediated actin nucleation, actin branch-formation, and *Listeria monocytogenes* motility. *J Cell Biol.* 2001;155(1):89–100.
106. Blackburn MR, Vance CO, Morschl E, Wilson CN. Adenosine receptors and inflammation. *Handb Exp Pharmacol.* 2009;(193):215–269.
107. Mills JH, Alabanza L, Weksler BB, Couraud PO, Romero IA, Bynoe MS. Human brain endothelial cells are responsive to adenosine receptor activation. *Purinergic Signal.* 2011;7(2):265–273.
108. Yu W, Zacharia LC, Jackson EK, Apodaca G. Adenosine receptor expression and function in bladder uroepithelium. *Am J Physiol Cell Physiol.* 2006;291(2):C254–C265.
109. Aliagas E, et al. Changes in expression and activity levels of ecto-5'-nucleotidase/CD73 along the mouse female estrous cycle. *Acta Physiol (Oxf).* 2010;199(2):191–197.
110. Mendoza-Rodriguez CA, Gonzalez-Mariscal L, Cerbon M. Changes in the distribution of ZO-1, occludin, and claudins in the rat uterine epithelium during the estrous cycle. *Cell Tissue Res.* 2005;319(2):315–330.